Science of the Total Environment 633 (2018) 12–29

Contents lists available at ScienceDirect

Science of the Total Environment

journal homepage: www.elsevier.com/locate/scitotenv

Comparing different methods for determining forest evapotranspiration and its components at multiple temporal scales

Qiang Tie [a,b], Hongchang Hu [a], Fuqiang Tian [a,*], N. Michele Holbrook [b]

[a] Department of Hydraulic Engineering, State Key Laboratory of Hydroscience and Engineering, Tsinghua University, Beijing 100084, China
[b] Department of Organismic and Evolutionary Biology, Harvard University, 16 Divinity Avenue, Cambridge, MA 02138, USA

HIGHLIGHTS

- Forest evapotranspiration (*ET*) is important for ecosystem-atmosphere water exchange.
- Methods for determining *ET* and its components were compared at four temporal scales.
- Sap flow-based *ET* estimate well agrees with eddy covariance-based estimate.
- Catchment water balance method may probably overestimate annual *ET*.
- Diurnal time lag effects exist between sap flow and eddy covariance-based estimates.

GRAPHICAL ABSTRACT

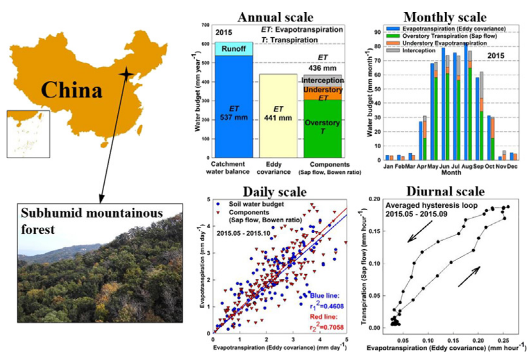

ARTICLE INFO

Article history:
Received 5 December 2017
Received in revised form 3 March 2018
Accepted 8 March 2018
Available online 20 March 2018

Editor: J Jay Gan

Keywords:
Forest evapotranspiration
Subhumid mountainous forest
Catchment water balance
Eddy covariance
Sap flow
Soil water budget

ABSTRACT

Accurately estimating forest evapotranspiration and its components is of great importance for hydrology, ecology, and meteorology. In this study, a comparison of methods for determining forest evapotranspiration and its components at annual, monthly, daily, and diurnal scales was conducted based on in situ measurements in the subhumid mountainous forest of North China. The goal of the study was to evaluate the accuracies and reliabilities of the different methods. The results indicate the following: (1) The sap flow upscaling procedure, taking into account diversities in forest types and tree species, produced component-based forest evapotranspiration estimate that agreed with eddy covariance-based estimate at the temporal scales of year, month, and day, while soil water budget-based forest evapotranspiration estimate was also qualitatively consistent with eddy covariance-based estimate at the daily scale; (2) At the annual scale, catchment water balance-based forest evapotranspiration estimate was significantly higher than eddy covariance-based estimate, which might probably result from non-negligible subsurface runoff caused by the widely distributed regolith and fractured bedrock under the ground; (3) At the sub-daily scale, the diurnal course of sap flow based-canopy transpiration estimate lagged significantly behind eddy covariance-based forest evapotranspiration estimate, which might physiologically be due to stem water storage and stem hydraulic conductivity. The results in this region may have much referential significance for forest evapotranspiration estimation and method evaluation in regions with similar environmental conditions.

* Corresponding author.
E-mail address: tianfq@tsinghua.edu.cn (F. Tian).

https://doi.org/10.1016/j.scitotenv.2018.03.082

Abbreviations

D discharge, m^3 $time^{-1}$
DBH tree diameter at breast height, cm
DH diameter of heartwood, cm
DS outer diameter of sapwood, cm
e vapor pressure, kPa
E_u evapotranspiration from the understory vegetation, including soil evaporation and the transpiration of the understory vegetation, mm $time^{-1}$
E_{u_b} E_u estimated from the Bowen ratio-energy balance method, mm $time^{-1}$
ET evapotranspiration from the entire ecosystem, mm $time^{-1}$
ET_{com} ET estimated as the sum of three evapotranspiration components ($E_{u\_b} + T_{o\_s} + I_d$), mm $time^{-1}$
ET_{cwb} ET estimated by the catchment water balance method, mm $time^{-1}$
ET_{ec} ET estimated by the eddy covariance method, mm $time^{-1}$
ET_{swb} ET estimated by the soil water budget method, mm $time^{-1}$
G ground heat flux, measured at a depth of 5 cm in the soil, W m^{-2}
H sensible heat flux estimated by the eddy covariance method, W m^{-2}
I interception loss of the overstory canopy, mm $time^{-1}$
I_d I estimated as the difference between precipitation and throughfall, mm $time^{-1}$
LAI leaf area index, obtained from a MODIS product (MCD15A3), m^2 m^{-2}
P precipitation, mm $time^{-1}$
P_t throughfall, mm $time^{-1}$
PAR photosynthetically active radiation, (μ)mol m^{-2} $time^{-1}$
Q_p energy flux associated with carbon dioxide flux (through photosynthesis and respiration), W m^{-2}
Q runoff, mm $year^{-1}$
R_n net radiation, W m^{-2}
RFA ratio of forest area to catchment area, km^2 km^{-2}
RFA_b RFA of broad-leaved forest, km^2 km^{-2}
RFA_m RFA of coniferous and broad-leaved mixed forest, km^2 km^{-2}
S rate of change in total heat storage of the forest air, water vapor, and biomass, W m^{-2}
S_a rate of change in heat storage forced by change in canopy air temperature, W m^{-2}
S_b rate of change in heat storage associated with the above-ground biomass, W m^{-2}
S_w rate of change in heat storage forced by change in canopy specific humidity, W m^{-2}
SA sapwood area, cm^2
SAI sapwood area index (ratio of sapwood area to ground area), cm^2 m^{-2}
SAI_{a_b} SAI of aspen (*Populus davidiana*) in broad-leaved forest, cm^2 m^{-2}
SAI_{a_m} SAI of aspen in coniferous and broad-leaved mixed forest, cm^2 m^{-2}
SAI_{l_m} SAI of larch (*Larix gmelinii*) in coniferous and broad-leaved mixed forest, cm^2 m^{-2}
SFD sap flux density, g cm^{-2} s^{-1}
SFD_a SA-weighted average SFD of all the experimental aspen trees, g cm^{-2} s^{-1}
SFD_l SA-weighted average SFD of all the experimental larch trees, g cm^{-2} s^{-1}
SWS soil water storage of the 0–850 mm soil layer, mm^3 mm^{-2}
T_a air temperature, °C
T_o transpiration from the overstory canopy, mm $time^{-1}$
T_{o_s} T_o upscaled from sap flow measurement, mm $time^{-1}$
VPD vapor pressure deficit, kPa
β Bowen ratio
γ psychrometric constant, kPa $°C^{-1}$
λE latent heat flux estimated by the eddy covariance method, W m^{-2}

1. Introduction

Forest evapotranspiration is one of the most significant factors influencing the terrestrial hydrological cycle (Jasechko et al., 2013; Oki and Kanae, 2006; Shimizu et al., 2015), and it is a major process that regulates water exchange between the forest ecosystem and the atmosphere (Cristiano et al., 2015). As the forest ecosystem generally consists of the overstory canopy and the understory vegetation, the evapotranspiration from the entire forest ecosystem (ET) is composed of three main components: the evapotranspiration from the understory vegetation (E_u), the transpiration from the overstory canopy (T_o), and the interception loss of the overstory canopy that is evaporated from the leaf surface (I), i.e.:

$$ET = E_u + T_o + I \tag{1}$$

Accurately estimating forest evapotranspiration and its components is of great importance for a wide range of disciplines, including hydrology, ecology, and meteorology, and is essential for understanding the links between the hydrological and ecologic systems of a forest (Good et al., 2015; Thompson et al., 2011a; Wei et al., 2017; Wilson et al., 2001). Several methods have been developed to estimate forest evapotranspiration and its components, and the corresponding spatial and temporal scales, and the estimated forest evapotranspiration components of the methods are quite different (Ford et al., 2007; Kosugi and Katsuyama, 2007; Oishi et al., 2008; Shimizu et al., 2015; Wilson et al., 2001; Yaseef et al., 2010). Generally, the catchment water balance method estimates catchment-scale $E_u + T_o + I$, and the sap flow method estimates individual tree-level T_o, and the soil water budget method estimates point-level $E_u + T_o$. In addition, the point-level I can be estimated individually from the difference between precipitation and throughfall (with the assumption of negligible stemflow). The spatial scales and the estimated components of the eddy covariance method and the Bowen ratio-energy balance method vary with the heights of the observation systems. When the observation systems are placed above the overstory canopy, regional-scale $E_u + T_o + I$ is estimated, and when the observation systems are placed under the overstory canopy but above the understory vegetation, small plot-scale E_u is estimated individually. The temporal scales of these methods are usually daily or sub-daily, while the catchment water balance method is generally only applied at the temporal scales longer than the annual cycle.

The spatial and temporal scale dependencies of the methods are significant, and each method is subject to certain limitations in applicability and accuracy (Thompson et al., 2011b; Wilson et al., 2001). The catchment water balance method generally provides no information on evapotranspiration processes at temporal scales shorter than the annual cycle or the individual evapotranspiration components, and the assumption of negligible bedrock infiltration may not be tenable under certain environmental conditions (Scott, 2010; Shimizu et al., 2015; Wilson et al., 2001). The application of the eddy covariance method in mountainous forests is difficult, and a series of corrections, including axis rotation for tilt correction, compensation for air density fluctuation, friction velocity filtering, etc., is needed (Etzold et al., 2010; Kosugi et al., 2007). The individual tree-level sap flow measurements need to be upscaled to the stand and catchment scales, while the diversities of forest types and tree species are rarely considered, leading to significant errors in the upscaled results (Ford et al., 2007; Oishi et al., 2008). The accuracies of the Bowen ratio-energy balance method and the soil water budget method are, to some extent, doubtful and unstable, and the data quality evaluation and control have to be conducted before application (Wilson et al., 2001; Zhang et al., 2008). The spatial variabilities in rainfall intensity and forest stand density markedly influence the accuracy of the interception loss of the overstory canopy estimated as the difference between precipitation and throughfall (Oishi et al., 2008). As a consequence, the applicability and accuracy of the methods used to determine forest evapotranspiration and its components need to be carefully evaluated.

Several studies have been conducted on the comparison of the different methods for determining forest evapotranspiration and its components, and the accuracies and reliabilities of the methods are analyzed and evaluated from different points of view (Cammalleri et al., 2013; Cristiano et al., 2015; Ford et al., 2007; Kosugi and Katsuyama, 2007; Oishi et al., 2008; Shimizu et al., 2015; Wang et al., 2015; Williams et al., 2004; Wilson et al., 2001; Yaseef et al., 2010). However, the evaluation results for the methods are not consistent in different studies, and some previous studies point out that the accuracy and reliability of the methods vary considerably with the environmental conditions (Shimizu et al., 2015; Wilson et al., 2001). Moreover, the comprehensive comparison of the methods at multiple spatial and temporal scales has seldom been conducted before.

In this study, a multi-method study was conducted to estimate forest evapotranspiration and its components in the subhumid earth-rock-mixed mountainous forest of North China (Peng et al., 2016; Sun et al., 2014; Tie et al., 2017; Zhao et al., 2015). The summary of the six methods used in the study is shown in Table 1, which also presents the estimated forest evapotranspiration components, the corresponding spatial and temporal scales, and the experimental periods of the methods. The six methods were systematically compared in this region at a spectrum of temporal scales ranging from annual, monthly, daily, and diurnal scales. The spatial scale transformation of the methods and the forest evapotranspiration partitioning at multiple temporal scales were also analyzed in depth. The main objectives of this study were: (1) to comprehensively evaluate the applicability and accuracy of the six methods for determining forest evapotranspiration and its components in this region at multiple temporal scales; and (2) to partition forest evapotranspiration into several components at multiple temporal scales and to analyze the proportions of the components, especially the transpiration ratio.

2. Materials and methods

2.1. Study site

Measurements were conducted in 2013–2015 in the Xitaizi Experimental Watershed (XEW, located at 40°32′ N and 116°37′ E, see Fig. 1), a subhumid mountainous catchment, approximately 70 km northeast of Beijing city in North China. The catchment area is 4.22 km^2, and the elevation ranges from 676 to 1201 m a.s.l.

XEW is characterized by a monsoon-influenced subhumid continental climate with a hot/humid summer and a cold/dry winter. According to the Miyun meteorological station (40°23′ N, 116°52′ E, 71.8 m a.s.l., 27 km southeast of XEW), long-term (25-year) mean annual air temperature, sunshine duration, relative humidity, and precipitation values are 11.5 °C, 2334.5 h, 59.1%, and 625.4 mm, respectively, while rain mainly occurs from June to September (~80% of the annual total) (Tie et al., 2017).

As a typical area of the earth-rock-mixed mountainous region of North China, XEW has pronounced characteristics in edaphic features, bedrock properties, and hydrologic conditions. The depth of soil layer is 0–1.5 m (depending on topography), and the soil is mainly classified as brown earth and cinnamon soil (in terms of Chinese soil taxonomy) (Tie et al., 2017). According to the field geological investigations conducted in XEW, the main bedrock type is granite (~88% of the total), while gneiss and dolomite are also sporadically distributed. Some parts of bedrock in XEW are fractured, and a layer of regolith is sandwiched between the soil layer and the bedrock layer under the ground. The groundwater table is 1.2–9.4 m below the ground surface (Tie et al., 2017).

XEW is surrounded and covered by mixed deciduous forest. The overstory canopy of the forest is dominated by aspen (*Populus davidiana*) and larch (*Larix gmelinii*), and the mean overstory canopy height is 12–13 m. As for the understory vegetation, annual plants grow thickly under the overstory canopy (with a height of 0–1.5 m), especially in summer.

2.2. Meteorological measurements and leaf area index observations

Four GRWS100 automatic weather stations (Campbell Scientific, Inc., Logan, UT, USA), named WS 1 to WS 4, were distributed out of the overstory canopy and uniformly along the altitude in XEW (their locations shown in Fig. 1), and meteorological conditions were continuously measured in 2013–2015. At each automatic weather station, air temperature (T_a) and relative humidity were measured by an HC2S3-L temperature and relative humidity probe (Rotronic AG, Grindelstrasse, Bassersdorf, Schweiz) with a radiation shield; photosynthetically active radiation (*PAR*) was measured by an LI-190R quantum sensor (LI-COR, Inc., Lincoln, NE, USA); and precipitation (*P*) was measured by a TE525 tipping bucket rain gauge (Texas Electronics, Inc., Dallas, TX, USA). The 10 min averages of the meteorological variables above were recorded on the CR1000 data loggers (Campbell Scientific, Inc., Logan, UT, USA). An integrated meteorological indicator, vapor pressure deficit (*VPD*) was calculated from the measured T_a and relative humidity (Norman and Campbell, 1998). In consideration of the representativeness for the whole catchment, the average meteorological values of the four automatic weather stations were used in the study.

Leaf area index (*LAI*) in 2013–2015 was acquired from Moderate Resolution Imaging Spectroradiometer (MODIS) *LAI* product (MCD15A3), instead of in situ measurement (Tie et al., 2017). Naithani et al. (2013) has pointed out that MODIS-derived *LAI* has good agreement with in situ-measured *LAI*, and is time- and cost-effective for the detection of temporal change in *LAI*. The spatial resolution of this remote sensing product is 1 km, and the temporal resolution is 4 d. Several data grids of MODIS *LAI* are contained in XEW, and their mean value was calculated in order to better reflect the overall *LAI* condition of XEW. The time series of MODIS original 4-d *LAI* was filtered with a Savitzky–Golay filtering procedure (Chen et al., 2004; Liu et al., 2013; Savitzky and Golay, 1964; Shen et al., 2011; Tie et al., 2017), and a smoothed daily series was then obtained and used in the study. The annual maximum *LAI* of XEW is 6.4 m^2 m^{-2}.

2.3. Sap flow measurements and upscaling procedures

According to a land use map of XEW and its surrounding area with a high spatial resolution of 1 m (see Fig. 1), which was interpreted from the high-resolution satellite remote sensing data of WorldView-2 commercial Earth observation satellite (DigitalGlobe, Inc., Westminster, CO, USA), the forest covers 98.6% of XEW, while the broad-leaved forest (75.1% of XEW), and the coniferous and broad-leaved mixed forest

Table 1
Summary of the methods used to estimate forest evapotranspiration and its components in this study (Wilson et al., 2001).

Method	Component	Spatial scale (m^2)	Temporal scale	Experimental period
Soil water budget	$E_u + T_o$	10^0	Daily	2013.08–2015.12
Difference between precipitation and throughfall	I	10^0	Daily	2014.08–2015.12
Sap flow (overstory)	T_o	10^2	Half-hour	2013.08–2013.11 2014.06–2014.10 2015.05–2015.10
Bowen ratio-energy balance (above the understory vegetation)	E_u	10^3	Half-hour	2014.08–2015.12
Eddy covariance (above the overstory canopy)	$E_u + T_o + I$	10^5	Half-hour	2014.08–2015.12
Catchment water balance	$E_u + T_o + I$	10^6	Annual	2013.09–2015.12

Shown are the methods, the components of evapotranspiration measured (T_o = transpiration of the overstory canopy; E_u = evapotranspiration from the understory vegetation, including soil evaporation and the transpiration of the understory vegetation; I = interception loss of the overstory canopy; the evapotranspiration from the whole forest ecosystem: $ET = E_u + T_o + I$), the approximate representative spatial scales of the measurement, the highest meaningful resolution temporal scales used to estimate evapotranspiration, and the experimental periods of the methods. Note that stemflow (the flow of intercepted water down the tree stem) and the interception loss of the understory vegetation are believed to be negligible for their much lower magnitudes, and they are not considered as independent components of evapotranspiration, and not measured directly in this study.

(22.6% of XEW) are the two main forest types. The land use map also shows that these two types of forest are distributed relatively uniformly in XEW and its surrounding area. In addition, a careful field survey of tree species was conducted all over the catchment, and it was found that the broad-leaved forest is dominated by aspen, and the coniferous and broad-leaved mixed forest is dominated by aspen and larch.

Many pre-existing studies pointed out that sap flow characteristics and sapwood area (*SA*) estimating empirical equations vary significantly with tree species (Bovard et al., 2005; Chen et al., 2011; Du et al., 2011; Oishi et al., 2008; Oren and Pataki, 2001; Small and McConnell, 2008; Wullschleger et al., 2001). Moreover, it is also obvious that tree species composition, stand density, and average tree basal area are different in different types of forest. In order to improve the accuracy and representativeness of sap flow-based canopy transpiration estimate in the mixed forest, the diversities of tree species and forest types were taken into consideration during the sap flow upscaling procedure in this study. In addition, Krauss et al. (2015b) also pointed out that the stand-level variability has significant influence on the accuracy of the sap flow upscaling procedure, and the plot sample size is quite important. Thus, two representative hillslopes in XEW were chosen as the study hillslopes, named SH 1 and SH 2 (their locations shown in Fig. 1), while SH 1 (north-facing, 780–805 m a.s.l.) is covered by typical broad-leaved forest consisting of a pure stand of aspen, and SH 2 (west-facing, 980–995 m a.s.l.) is covered by typical coniferous and broad-leaved mixed forest consisting of a mixed stand of aspen and larch. Several trees of these two species with different diameter at breast height (*DBH*) were selected as experimental trees for sap flow measurements in SH 1 and SH 2 during the growing seasons of 2013–2015, while the details concerning the numbers of experimental trees are shown in Table 2.

Sap flow was measured using thermal dissipation probes (TDPs) (Dynamax, Inc., Houston, TX, USA). Three different-sized probes (TDP10, TDP30, TDP50, with lengths of 10 mm, 30 mm, and 50 mm,

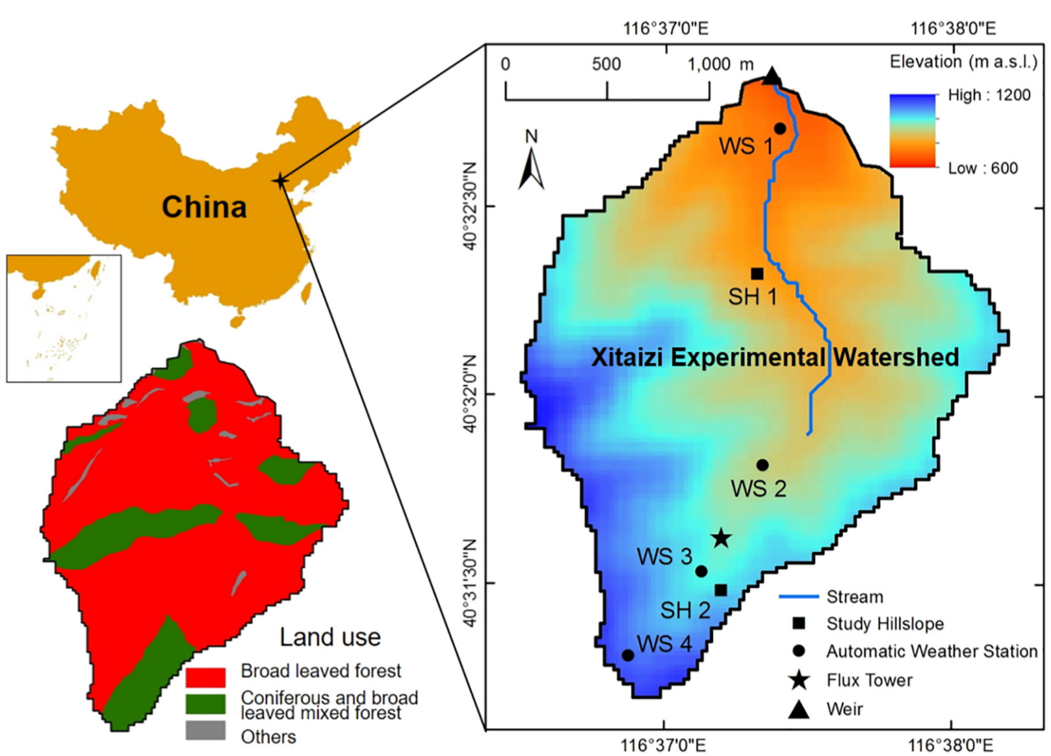

Fig. 1. Location, elevation, land use, and experiment configuration of the Xitaizi Experimental Watershed.

Table 2
General physiological parameters, empirical equations established to estimate sapwood area, and sap flow measurement information for aspen (*Populus davidiana*) and larch (*Larix gmelinii*) in the Xitaizi Experimental Watershed.

Tree species		Aspen (*Populus davidiana*)	Larch (*Larix gmelinii*)
Mean tree height[a] (m)		12.1	12.9
Mean crown width[a] (m)		4.2	5.0
Linear regression equation to estimate *DH*[b]		$DH = 0.5072 \times DBH - 0.5889$ ($r^2 = 0.9655, n = 13$)	$DH = 0.6391 \times DBH - 0.5886$ ($r^2 = 0.9328, n = 9$)
Linear regression equation to estimate *DS*[b]		$DS = 0.9453 \times DBH - 0.4412$ ($r^2 = 0.9948, n = 13$)	$DS = 0.8787 \times DBH + 0.4932$ ($r^2 = 0.9945, n = 9$)
Equation to calculate *SA*		$SA = \frac{\pi}{4} \times (DS^2 - DH^2)$	$SA = \frac{\pi}{4} \times (DS^2 - DH^2)$
Number of experimental trees used for sap flow measurement[c]	2013	5 (SH 1)	
	2014	7 (SH 1), 3 (SH 2)	3 (SH 2)
	2015	6 (SH 1), 3 (SH 2)	3 (SH 2)

DBH, *DH*, *DS*, and *SA* denote tree diameter at breast height, diameter of heartwood, outer diameter of sapwood, and sapwood area, respectively.
[a] General physiological parameters of tree species were acquired from the sample plot investigations conducted in the study hillslopes in the Xitaizi Experimental Watershed in 2014.
[b] The linear regression equations were established by cutting down 13 aspen and 9 larch trees with different *DBH* in an adjacent region near the Xitaizi Experimental Watershed with similar environmental conditions in 2014, measuring their *DBH*, *DH*, and *DS*, and then conducting linear regression analyses.
[c] The locations of the study hillslopes SH 1 and SH 2 are marked in Fig. 1.

respectively) were used in this study to match the sapwood width of the experimental trees with different *DBH*. All probes were uniformly installed on the south side of the corresponding tree trunks at approximately 1.1 m above the land surface. A probe set consists of two needles, a heated one above and a reference one below. The two needles were inserted into the sapwood about 0.15 m apart vertically. The temperature difference between them was measured, and 10 min averages were recorded on the CR1000 data loggers. Sap flux density (*SFD*) was then calculated from the temperature difference between the two needles using the empirical relationship established by Granier (1987). More details concerning the sap flow measurements in XEW, and the mechanism and the installation procedure of thermal dissipation probe are provided by Tie et al. (2017).

Thirteen aspen and nine larch trees with different *DBH* in an adjacent region near XEW with similar environmental conditions were cut down in 2014, and their *DBH*, diameter of heartwood (*DH*), and outer diameter of sapwood (*DS*) were measured. The *SA* estimating empirical equations were then established respectively for aspen and larch by conducting linear regression analyses, and are presented in Table 2 in detail. Furthermore, careful sample plot investigations were conducted in SH 1 (the representative of broad-leaved forest) and SH 2 (the representative of coniferous and broad-leaved mixed forest) in XEW in 2014. The general physiological parameters of the two tree species, and the tree species composition (including the percentage of tree species) of the two forest types were then acquired, and are respectively shown in Tables 2 and 3. The stand densities and the average *DBH* of the two tree species in the two types of forest were also respectively investigated during the sample plot investigations in SH 1 and SH 2. Therefore, based on the *SA* estimating empirical equations and the forest stand parameters, sapwood area indexes (*SAI*), namely the ratios of *SA* to ground area, were calculated respectively for the two tree species in the two types of forest, and are shown in Table 3. Moreover, the ratios of forest area to catchment area (*RFA*) respectively for the two types of forest are also shown in Table 3.

Using the *SA* estimating empirical equations in Table 2, the *SA* of the experimental trees was calculated from the measured *DBH*. The *SA*-weighted average *SFD* of the experimental trees was then calculated respectively for the two tree species in order to eliminate the impact of *SFD* variability among different experimental trees, and to represent the *SFD* of the tree species better. Combining the *SA*-weighted average *SFD* of the two tree species, the *SAI* of the two tree species in the two types of forest, and the coverage rate of the two forest types in XEW, a sap flow upscaling procedure aiming at mixed forest canopy transpiration estimate was established. In this study, the parts of XEW not covered by these two types of forest, and the other tree species in the forest were assumed to be negligible, and not considered in the sap flow upscaling procedure, because of their too small occupation area. Transpiration of the overstory canopy (T_o) was then calculated as follows:

$$T_{o\_s} = SFD_a \times SAI_{a\_b} \times RFA_b + (SFD_a \times SAI_{a\_m} + SFD_l \times SAI_{l\_m}) \times RFA_m \quad (2)$$

where T_{o_s} is the T_o upscaled from sap flow measurement (mm day^{-1}), SFD_a and SFD_l are respectively the *SA*-weighted average *SFD* of all the experimental trees of aspen and larch (mm day^{-1}), SAI_{a_b} is the *SAI* of aspen in broad-leaved forest (m^2 m^{-2}), SAI_{a_m} and SAI_{l_m} are respectively the *SAI* of aspen and larch in coniferous and broad-leaved mixed forest (m^2 m^{-2}), and RFA_b and RFA_m are respectively the *RFA* of broad-leaved forest and coniferous and broad-leaved mixed forest (km^2 km^{-2}).

2.4. Eddy covariance and energy balance measurements

A 30 m-height over-canopy flux tower was built in XEW, and its location is shown in Fig. 1. The elevation of the tower base is 974 m a.s.l. Two eddy covariance systems were mounted on the flux tower and used in the study, while one system was positioned 15 m above the forest floor (a little higher than canopy height), and the other one was positioned 30 m above the forest floor (a little higher than twice canopy height). Eddy covariance measurements were then continuously conducted in 2014–2015 simultaneously by the two systems in order to validate the applicability and reliability of eddy covariance method in such mountainous mixed forest region. Each eddy covariance system on the flux tower was comprised of a CSAT3 three-dimensional, ultrasonic anemometer (Campbell Scientific, Inc., Logan, UT, USA) and an EC150 CO_2/H_2O open-path, mid-infrared absorption gas analyzer (Campbell Scientific, Inc., Logan, UT, USA). The three components of the wind velocity vector, sonic temperature, and scalar concentrations of water vapor and carbon dioxide were sampled at 10 Hz and recorded on the CR3000 data loggers (Campbell Scientific, Inc., Logan, UT, USA).

As recommended by several previous studies (Chi et al., 2016; Fortuniak et al., 2017; Heusinger and Weber, 2017; Mitchell et al., 2015; Zhang et al., 2016; Zhou et al., 2017; Ziemblińska et al., 2016), the raw 10 Hz eddy covariance data were processed using EddyPro software version 6.1.0 (LI-COR, Inc., Lincoln, NE, USA) to produce half-hourly fluxes of latent heat (λE), sensible heat (H), water vapor (ET), and carbon dioxide with the eddy covariance method. During the data processing procedures by EddyPro software, axis rotation for tilt correction, block averaging, humidity correction of sonic temperature, compensation for air density fluctuation, compensation for time lag, statistical test, and spectral correction were performed on the half-

Table 3
Characteristics of sap flow measurement plots in the Xitaizi Experimental Watershed.

Forest type	Broad-leaved forest	Coniferous and broad-leaved mixed forest
RFA[a]	$RFA_b = 75.1\%$	$RFA_m = 22.6\%$
Dominant tree species[b]	Aspen (*Populus davidiana*), ~98%	Aspen, ~72% Larch (*Larix gmelinii*), ~27%
SAI[c]	$SAI_{a\_b} = 17.77\ cm^2\ m^{-2}$	$SAI_{a\_m} = 14.86\ cm^2\ m^{-2}$ $SAI_{l\_m} = 3.67\ cm^2\ m^{-2}$
Representative study hillslope[d]	SH 1 (slope: 45%; soil depth: 1.2–1.5 m)	SH 2 (slope: 36%; soil depth: 0.8–1.0 m)

RFA denotes ratio of forest area to catchment area, and RFA_b and RFA_m denote *RFA* of broad-leaved forest, and *RFA* of coniferous and broad-leaved mixed forest, respectively. *SAI* denotes sapwood area index (ratio of sapwood area to ground area), and SAI_{a_b}, SAI_{a_m}, and SAI_{l_m} denote *SAI* of aspen in broad-leaved forest, *SAI* of aspen in coniferous and broad-leaved mixed forest, and *SAI* of larch in coniferous and broad-leaved mixed forest, respectively.

[a] *RFA* was acquired from a land use map of the Xitaizi Experimental Watershed with a high spatial resolution of 1 m (see Fig. 1), which was interpreted from the high-resolution satellite remote sensing data of WorldView-2 commercial Earth observation satellite (DigitalGlobe, Inc., Westminster, CO, USA).

[b] Percentage of dominant tree species in the forest was acquired from the sample plot investigation conducted in the corresponding study hillslope in the Xitaizi Experimental Watershed in 2014.

[c] *SAI* was calculated from the stand density and the average diameter at breast height (*DBH*) acquired from the sample plot investigation conducted in the corresponding study hillslope in the Xitaizi Experimental Watershed in 2014, while sapwood area (*SA*) estimating empirical equations in Table 2 were used in the calculation process to acquire *SA* from *DBH*.

[d] The locations of the study hillslopes SH 1 and SH 2 are marked in Fig. 1.

hourly eddy covariance flux data (Foken et al., 2004; Mauder et al., 2013; Moncrieff et al., 2004; Moncrieff et al., 1997; Van Dijk et al., 2004; Vickers and Mahrt, 1997; Webb et al., 1980). The corrected flux data was then filtered by the friction velocity threshold using the REddyProcWeb online tool developed by the Max Planck Institute for Biogeochemistry (see http://www.bgc-jena.mpg.de/REddyProc/brew/REddyProc.rhtml). The friction velocity threshold was not fixed, but estimated by the Moving Point Test according to Papale et al. (2006). The percentages of the data filtered out were 31% and 25% respectively for 15-m and 30-m eddy covariance systems. The fragmented quality-controlled flux data was then gap-filled also using the REddyProcWeb online tool, which implemented the standardized eddy covariance gap-filling methods of Reichstein et al. (2005), and continuous time series of half-hourly fluxes of λE, *H*, *ET*, and carbon dioxide were then acquired.

Meanwhile, two CNR4 net radiometers (Kipp & Zonen B.V., Delft, Netherlands) were mounted on the flux tower at the heights of 15 m and 30 m, respectively corresponding to the two eddy covariance systems. The energy balance between incoming and outgoing radiation was continuously measured during the eddy covariance measurements, and 10 min averages were recorded on the CR1000 data logger. As suggested by Hammerle et al. (2007) and Wohlfahrt et al. (2016), a slope-terrain correction was conducted on the measured incoming shortwave radiation. Then, the net radiations (R_n) at the heights of 15 m and 30 m were respectively calculated. Ground heat flux (*G*) was also continuously measured during the eddy covariance measurements by six HFP01SC self-calibrating heat flux sensors (Hukseflux Thermal Sensors B.V., Delft, Netherlands), which were installed at the depth of 5 cm in the soil, and distributed in SH 1 (three sensors) and SH 2 (three sensors) in consideration of representativeness. The 30 min averages of *G* were recorded on the CR1000 data loggers, and the average *G* of the six heat flux sensors was used in the study.

As suggested by Barr et al. (2006), Kosugi et al. (2007), and Silberstein et al. (2001), in order to more accurately calculate and evaluate the energy balance closures of the eddy covariance measurements, the heat storage of the forest air, water vapor, and biomass between the eddy covariance measurement height and ground surface was also continuously monitored along with the eddy covariance measurements. Seven HC2S3-L temperature and relative humidity probes with radiation shields were mounted on the flux tower respectively at the heights of 2, 5, 10, 15, 20, 25, and 30 m, and T_a and relative humidity were measured at each height. An SI-111 infrared radiometer (Apogee Instruments, Inc., Logan, UT, USA) was mounted on the flux tower at the heights of 5 m, and the tree trunk surface temperature was measured, which was approximatively treated as the tree trunk temperature in this study. In addition, barometric pressure was measured by a CS100 standard barometer (Campbell Scientific, Inc., Logan, UT, USA) mounted on the flux tower at the height of 2 m. The 10 min averages of the variables above were recorded on the CR1000 data loggers. Based on the T_a and relative humidity measurements at seven different heights and the barometric pressure measurement, average T_a and average specific humidity were calculated respectively for 0–15 m and 0–30 m, and the rate of change in heat storage forced by change in canopy air temperature (S_a) and the rate of change in heat storage forced by change in canopy specific humidity (S_w) were then calculated also respectively for 0–15 m and 0–30 m (Barr et al., 2006; Blanken et al., 1997; Kosugi et al., 2007). The rate of change in heat storage associated with the above-ground biomass (S_b) was roughly estimated from the measured tree trunk temperature and the forest information acquired from the sample plot investigations (Barr et al., 2006; Blanken et al., 1997; Kosugi et al., 2007). Then, the rate of change in total heat storage of the forest air, water vapor, and biomass between the eddy covariance measurement height and ground surface (*S*) was calculated as follows:

$$S = S_a + S_w + S_b \tag{3}$$

2.5. Catchment water balance measurements

A concrete weir with a grit chamber was built on the stream at the outlet of XEW (its location shown in Fig. 1), and a Parshall flume was installed in the center of the weir. The water level in the flume was continuously measured and recorded at 10 min intervals in 2013–2015 by a HOBO U20-001-04 water level data logger (Onset Computer Corp., Bourne, MA, USA), and the correction was conducted on the measured water level with the water level simultaneously measured by the staff gauge with the naked eye at a much lower frequency. The instantaneous discharge from XEW (*D*) was then calculated from the corrected water level using the empirical formula of the Parshall flume, and annual *D* was calculated by summing the 10 min readings over the year. Annual runoff (*Q*) was calculated by dividing annual *D* by the surface area of the entire catchment (4.22 km^2). Annual *P* was also calculated by summing the 10 min readings over the year. Many previous studies indicated that, at annual or multi-year scale, the net change in the water storage of the whole catchment is negligible when compared with the total values of *P*, *Q*, and evapotranspiration (Ford et al., 2007; Kosugi and Katsuyama, 2007; Shimizu et al., 2015; Wang et al., 2015; Wilson et al., 2001). Therefore, the catchment water balance method was conducted at annual scale in this study, and annual evapotranspiration integrated over the entire catchment (*ET*) was then estimated as the residual between annual *P* and annual *Q* under the assumption of negligible net annual change in catchment water storage, i.e.:

$$ET_{cwb} = P - Q \tag{4}$$

where ET_{cwb} is the *ET* estimated from the catchment water balance method.

2.6. Soil water budget measurements

Soil water budget measurements were conducted in XEW in 2013–2015, and evapotranspiration ($E_u + T_o$) was then estimated from the measurements with several assumptions (Cuenca et al., 1997; Oren et al., 1998; Wilson et al., 2001). In view of the high spatial variability of soil water, eight vertical soil profiles for soil water budget measurements were set up, and distributed in SH 1 (five soil profiles) and SH 2 (three soil profiles). A careful field survey of tree root distributions along the vertical soil profiles was conducted in XEW, and showed that the majority of the root systems of aspen and larch were distributed in the top 800 mm soil layer, while the fine roots were mostly found in the top 600 mm. Several previous studies also pointed out that the effective depth of the soil layer for soil evaporation is generally quite shallow (100–150 mm) (Allen et al., 2005; Wilson et al., 2001). Therefore, no soil water was assumed to contribute to transpiration and soil evaporation from the soil layer below 850 mm in this study, and soil water budget measurements were conducted in the 0–850 mm soil layer. In each of the eight vertical soil profiles, eight CS616 water content reflectometers (Campbell Scientific, Inc., Logan, UT, USA) were installed respectively at soil depths of 100, 200, 300, 400, 500, 600, 700, and 800 mm, and the volumetric soil water content was continuously monitored at each soil depth based on the time-domain reflectometry (TDR) technique. The 10 min averages of the soil water content were recorded on the CR1000 data loggers.

The measured soil water contents at these eight soil depths were assumed to be representative for the surrounding soil layers and were applied to the corresponding soil depths of 0–150, 150–250, 250–350, 350–450, 450–550, 550–650, 650–750, and 750–850 mm, respectively, and soil water storage (*SWS*) of 0–850 mm soil layer was then calculated by integrating the soil water contents of eight soil layers along soil depth. The average *SWS* for all the profiles was calculated and used in the study in order to reduce the influences of the high spatial variability of soil water and the lateral flow as much as possible. Daily evapotranspiration ($E_u + T_o$) was estimated as daily total water loss from the soil, i.e., daily decrease in *SWS*. As recommended by Wilson et al. (2001), the calculated evapotranspiration results of all days with rain and up to two additional days following heavy rain events were eliminated, because rain inputs, downward movements of soil water within the soil profiles and possible deep drainage losses confounded estimates of soil water extraction using the soil water budget approach. Furthermore, the evapotranspiration results during the snowmelt period in spring were also eliminated for similar reason. Annual or monthly evapotranspiration totals were not attempted based on the soil water budget method in the study in consideration of the large amount of missing data.

2.7. Bowen ratio-energy balance measurements

Bowen ratio-energy balance measurements were also conducted via the flux tower, and evapotranspiration from the understory vegetation (E_u), including soil evaporation and the transpiration of the understory vegetation, was estimated using the Bowen ratio-energy balance method (Nagler et al., 2005; Zhang et al., 2008). In consideration of the heights of both overstory canopy and understory vegetation, T_a and relative humidity measured at 2-m and 5-m heights, which were under the overstory canopy but above the understory vegetation, were used, and vapor pressure (e) was calculated respectively for the two heights. The Bowen ratio (β) was then calculated from the vertical gradients of T_a and e as follows:

$$\beta = \gamma \frac{\Delta T_a}{\Delta e} \tag{5}$$

where ΔT_a and Δe are respectively the T_a and e differences between the two heights, and γ is the psychrometric constant. Note that the extremely strict calibrations were conducted for the two temperature and relative humidity probes used for Bowen ratio-energy balance measurements every three months during the measurements with the help of the engineers from the instrument supplier, because the calculation of Bowen ratio is quite sensitive to the errors in air temperature and vapor pressure, especially the relative error between the two probes.

As the R_n above the overstory canopy was measured by the flux tower, the R_n below the overstory canopy was estimated from the R_n above the overstory canopy, *LAI*, and solar zenith angle using the Beer-Lambert law (Friedl, 1996; Murray and Verhoef, 2007; Nagler et al., 2005; Sonohat et al., 2004), and λE was then calculated as follows:

$$\lambda E = \frac{R_n - G}{1 + \beta} \tag{6}$$

where R_n is below the overstory canopy. The quality control was conducted on the calculated λE according to Perez et al. (1999) and Zhang et al. (2008) in order to ensure the reliability and precision of λE, and then E_u was calculated from λE.

2.8. Measurements of difference between precipitation and throughfall

Throughfall (P_t) was continuously measured in 2014–2015 by five TE525 tipping bucket rain gauges mounted under the overstory canopy but above the understory vegetation, which were distributed in SH 1 (four rain gauges) and SH 2 (one rain gauge) in consideration of representativeness. The 10 min averages of P_t were recorded on the CR1000 data loggers, and the average P_t of the five rain gauges was used in the study. Many previous studies pointed out that stemflow is generally a small percentage (<5%) of total precipitation (Levia and Germer, 2015; Wei et al., 2005). Oishi et al. (2008) conducted an exploratory investigation on the proportion of precipitation reaching the forest floor as stemflow over a 2-month period with varying *LAI* in a hardwood forest region with climatic and stand condition similar to XEW, and drew a conclusion that stemflow is negligible for its much lower magnitude. The previous studies conducted in the subhumid earth-rock-mixed mountainous forest of North China also indicated that the proportion of stemflow to the total precipitation is only 1–5% (Hu et al., 2010; Liang et al., 2012; Xiao et al., 2007). Therefore, stemflow was neglected in this study, and interception loss of the overstory canopy (I) was then estimated as the residual between P and P_t.

3. Results and discussion

3.1. Energy balance closure and variations in hydrologic and meteorological factors

Energy balance closure is widely used to evaluate the reliability and the accuracy of eddy covariance measurements (Heusinger and Weber, 2017; Williams et al., 2004; Wilson et al., 2002; Zhang et al., 2014). As pointed out by many previous studies (Kosugi et al., 2007; Scott, 2010; Silberstein et al., 2001; Wilson et al., 2002), the surface energy balance can be written as follows:

$$\lambda E + H = R_n - G - S - Q_p \tag{7}$$

where Q_p is the energy flux associated with carbon dioxide flux through photosynthesis and respiration, which has been estimated from the measured carbon dioxide flux (Barr et al., 2006; Blanken et al., 1997) in this study. The imbalance between the independently measured terms on the left- and right-hand sides of the equation may indicate the inaccurate estimates of scalar fluxes.

In order to detect the energy balance closure of eddy covariance measurements, the scatter plots of half-hourly $\lambda E + H$ against $R_n - G - S - Q_p$ respectively for 15-m and 30-m eddy covariance systems are depicted in Fig. 2A and B, and the data of the whole year of 2015 (totally 17,520 data points) are plotted. Linear regression analyses were conducted between $\lambda E + H$ and $R_n - G - S - Q_p$ respectively for the two eddy covariance systems (see Fig. 2A and B for detailed results). The slopes of the regression lines are 0.8849 ($r^2 = 0.8388$) and 0.8965 ($r^2 = 0.8012$) respectively for 15-m and 30-m eddy covariance systems, indicating satisfactory energy balance closures of both eddy covariance systems, as the energy balance closures generally range from 0.7 to 0.9 in the previous studies conducted in the similar mountainous forest regions (Iida et al., 2009; Kosugi et al., 2007; Kumagai et al., 2005; Shimizu et al., 2015; Wilson et al., 2001). Stoy et al. (2006) and Wilson et al. (2002) summarized the primary reasons usually suspected for the energy imbalance in the eddy covariance measurement, among which, for this study, the systematic errors associated with the sampling mismatch between the eddy covariance flux footprint and the sensors measuring other components of the surface energy balance (such as net radiation and ground heat flux), and the difficulty in accurately estimating the rate of change in heat storage between the eddy covariance measurement height and ground surface, might primarily account for the slight energy imbalances of both eddy covariance systems. Scott (2010) also pointed out that the justification for the energy imbalance correction is ambiguous at seasonal to annual scales, for it may lead to worse results. Therefore, the energy imbalances in this study might not mainly result from the errors in the eddy covariance measurements, and the energy imbalance correction was not conducted on the eddy covariance fluxes, just the same with many previous studies (Chi et al., 2016; Iida et al., 2009; Mitchell et al., 2015; Oishi et al., 2008; Sun et al., 2008; Williams et al., 2004; Wilson et al., 2001; Yaseef et al., 2010; Zhang et al., 2014; Zhou et al., 2017). Thus, the flux of water vapor, i.e. *ET*, without energy imbalance correction, was used in the later analyses.

To further evaluate the reliability and representativeness of eddy covariance measurements in XEW, the comparison of daily *ET* estimates (ET_{ec}) from 15-m and 30-m eddy covariance systems is scatter-plotted in Fig. 2C, and the data of the whole year of 2015 (totally 365 data points) are plotted. Linear regression analysis was conducted between ET_{ec} from 15-m and 30-m eddy covariance systems (see Fig. 2C for detailed results). The slope of the regression line is 0.9495 ($r^2 = 0.9453$), indicating quite good agreement between ET_{ec} from 15-m and 30-m eddy covariance systems. The annual ET_{ec} from 15-m and 30-m eddy covariance systems without and with the energy imbalance correction in 2015 were also respectively calculated. The annual ET_{ec} from 15-m eddy covariance system in 2015 was 464 mm without the energy imbalance correction, and 524 mm with the energy imbalance correction, while the annual ET_{ec} from 30-m eddy covariance system in 2015 was 441 mm without the energy imbalance correction, and 492 mm with the energy imbalance correction. There were still some differences between the annual ET_{ec} without and with the energy imbalance correction both for 15-m and 30-m eddy covariance systems. Thus, although ET_{ec} without energy imbalance correction was used in the later analyses, the energy imbalance of the eddy covariance measurements should also be considered as an important possible error source in the study. In addition, footprint analyses were conducted respectively for 15-m and 30-m eddy covariance systems using the footprint models established by Kljun et al. (2004) and Kormann and Meixner (2001). For 15-m eddy covariance system, 90% of the flux originated from <90 m around the flux tower, and for 30-m eddy covariance system, 90% of the flux originated from <350 m around the flux tower. Thus, the flux footprint of 30-m eddy covariance system was much larger than that of 15-m eddy covariance system, while the stand density around the flux tower is a little higher in comparison to the average value of XEW according to field observations, which brought about the result that ET_{ec} from 15-m eddy covariance system was a little higher than that from 30-m eddy covariance system on average, and the slope of the regression line was lower than 1 slightly.

The satisfactory energy balance closures and the good agreement between two eddy covariance systems both gave much confidence in the eddy covariance measurements in this study. The good agreement between two eddy covariance systems also implied that the fluxes from different footprints were quite consistent in XEW, confirming that different types of forest are distributed relatively uniformly in XEW, and eddy covariance measurements are quite representative for the whole catchment. This laid the foundation for the comparability of ET_{ec} and ET_{cwb}. As the footprint of 30-m eddy covariance system matched the area of XEW better, ET_{ec} from 30-m eddy covariance system could reflect the entire ecosystem evapotranspiration of XEW better, and was used in the later analyses. However, considering the differences between ET_{ec} from 15-m and 30-m eddy covariance systems, the footprint of the eddy covariance measurements should also be considered as an important possible error source for the estimate of *ET* from entire XEW using eddy covariance measurements in the study.

In order to give a general overview of variations in measured hydrologic and meteorological factors in this study, seasonal variations in the daily values of *D*, *P*, and *SWS* in 2013, 2014 and 2015 are shown in Fig. 3, and seasonal variations in the daily values of *LAI*, *PAR*, T_a, *VPD*, T_{o_s}, and *ET* estimates from soil water budget (ET_{swb}) in 2013, 2014 and 2015 are shown in Fig. 4. The results showed significant responses of *D* and *SWS* to *P*. The net change in *SWS* throughout the year of 2014 was 4.5 mm, and it was 9.5 mm throughout the year of 2015, indicating that the net change in *SWS* was negligible at annual scale. T_{o_s} exhibited similar seasonal trend with *LAI*, while the day-to-day fluctuations in T_{o_s} were much larger. Tie et al. (2017) pointed out that *PAR* is identified as the key environmental factor controlling sap flow in the subhumid earth-rock-mixed mountainous region of North China. In this study, T_{o_s} also showed daily variations quite similar to those of *PAR*, further verifying that *PAR* was a dominant control of tree transpiration. The data points of ET_{swb} were discontinuous, as the data points, which did not meet the assumptions of the soil water budget method, had been eliminated. However, daily and seasonal variations in ET_{swb} could roughly match those of T_{o_s}, and the two estimates were qualitatively similar.

3.2. Comparisons at the annual scale

In this study, annual *ET* was mainly estimated from the catchment water balance method (ET_{cwb}) and the eddy covariance method (ET_{ec}). As annual T_o was upscaled from sap flow measurement (T_{o_s}), annual E_u was estimated from the Bowen ratio-energy balance method (E_{u_b}), and annual *I* was estimated as the difference between precipitation and throughfall (I_d), annual *ET* could also be estimated as the sum of these three *ET* components ($ET_{com} = E_{u\_b} + T_{o\_s} + I_d$). Fig. 5 shows these three independent estimates of annual *ET*, i.e., ET_{cwb} (2014 and 2015), ET_{ec} (2015), and ET_{com} (2015), and the *ET* components estimates are also shown. Annual ET_{ec} and ET_{com} in 2014 were not acquired because of the incomplete experimental data.

The catchment water balance method was conducted in both 2014 and 2015. The *P* and *Q* in 2015 were both lower than those in 2014, while ET_{cwb} was slightly higher in 2015. Many previous studies noted that the net annual change in catchment water storage is negligible when compared with the values of *P*, *ET*, and *Q* (Ford et al., 2007; Kosugi and Katsuyama, 2007; Shimizu et al., 2015; Wang et al., 2015; Wilson et al., 2001). As indicated in Section 3.1, the net annual changes in *SWS* were 4.5 mm in 2014 and 9.5 mm in 2015, which were orders of magnitude less than *P*, *ET*, and *R*. Therefore, the net annual change in catchment water storage was not taken into consideration in the catchment water balance method in this study. However, *SWS* only represented the soil water storage of the shallow soil layer (0–850 mm), and the net annual changes in soil water storage of deep soil layer and groundwater storage are still unknown, which might be a source of error in the ET_{cwb} calculation.

As shown in Fig. 5, according to the annual *ET* results in 2015, ET_{com} (436 mm) has quite good agreement with ET_{ec} (441 mm), while ET_{cwb} (537 mm) is obviously higher when compared with ET_{ec} and ET_{com}. As these three estimates of annual *ET* were independently acquired by three different methods, the strong agreement between ET_{com} and ET_{ec}, along with the satisfactory energy balance closure of eddy covariance measurement, provided confidence in the accuracies of both ET_{com} and ET_{ec}, while ET_{cwb} was then believed likely to markedly overestimate annual *ET*.

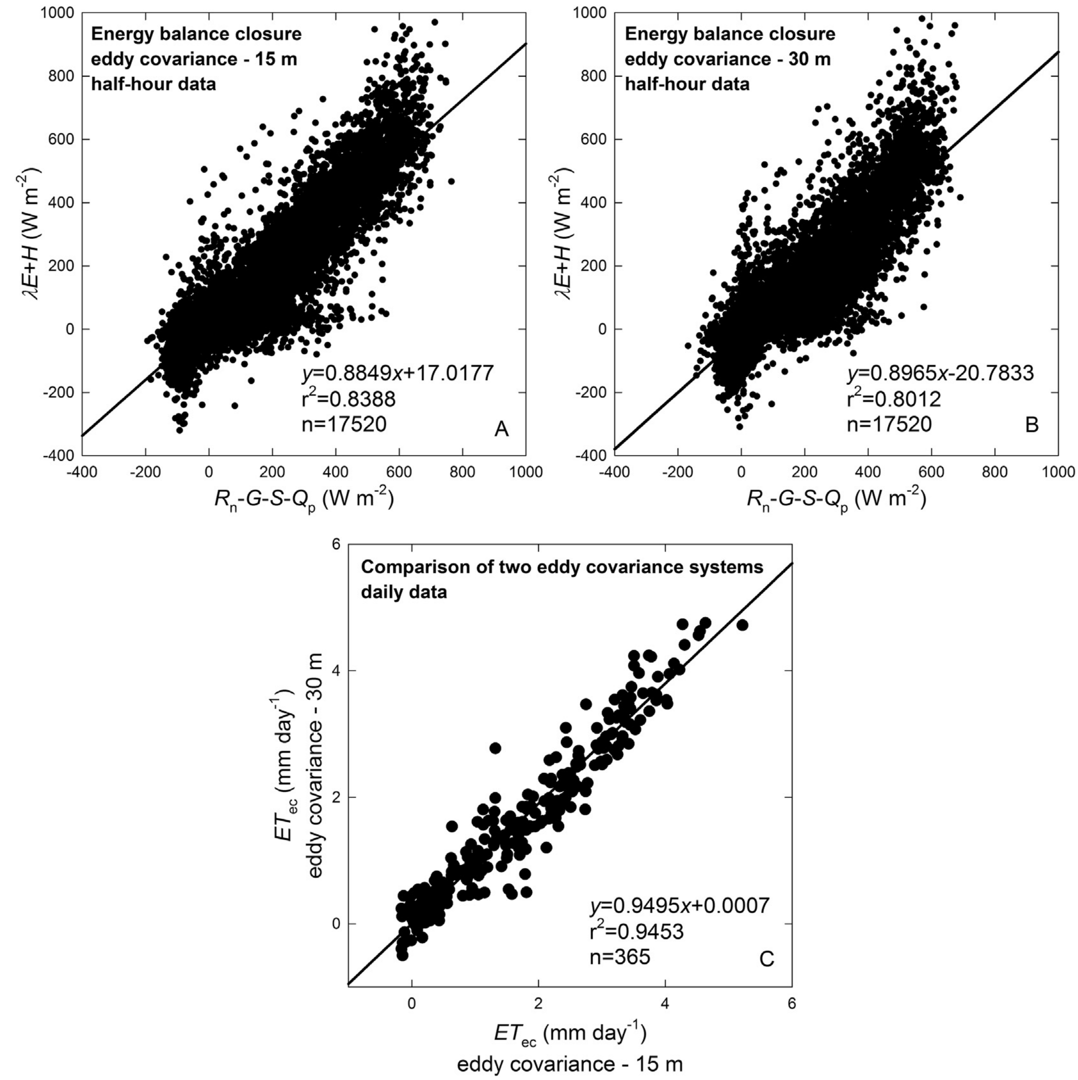

Fig. 2. Energy balance closures (the sum of latent and sensible heat flux by eddy covariance ($\lambda E + H$) against the residual of net radiation minus ground heat flux, rate of change in heat storage of forest, and energy flux associated with carbon dioxide flux ($R_n - G - S - Q_p$)) respectively for (A) 15 m and (B) 30 m height eddy covariance systems, and (C) comparison of entire ecosystem evapotranspiration estimates (ET_{ec}) from 15 m and 30 m height eddy covariance systems. Data are paired half-hourly averages in (A) and (B), and daily averages in (C), and all the data obtained in 2015 are plotted. Regression lines, regression equations, coefficients of determination (r^2), and numbers of data (n) are also shown.

Several previous studies have already compared different methods for determining annual ET and its components in forest regions, and some evaluations have been made for the accuracy of the methods, while no consistent conclusion has been drawn, and the applicability of the methods varies with environmental conditions significantly. The results of annual estimates of ET and its components from six representative studies conducted in comparable forests are summarized and presented in Table 4, and are compared with the results of this study. Most of these studies considered ET_{cwb} as the most reliable annual ET estimate, and used ET_{cwb} to evaluate the validities of other estimation methods. However, Ford et al. (2007), Shimizu et al. (2015), and Wilson et al. (2001) also pointed out that the catchment water balance method is subject to the errors based on the assumptions that bedrock infiltration, deep drainage, annual change in catchment water storage, and groundwater flow contributions to runoff are negligible. They suggested that the catchment water balance method should be examined carefully for its applicability, prior to the use in a particular catchment. As for ET_{ec} and ET_{com}, most of these studies indicated that ET_{ec} had good agreement with ET_{cwb}, which was thought to validate the accuracies of both methods, while ET_{com} was generally considered to tend to underestimate ET when compared with ET_{cwb} and ET_{ec}. Wilson et al. (2001) suggested that ET_{com} underestimated ET by 16–28% (compared with ET_{cwb}), and Ford et al. (2007) suggested that ET_{com} underestimated ET by 7–14% (compared with ET_{cwb}). However, Wilson et al. (2001) also pointed out that sap flow-based ET estimate has some unique advantages in estimating water use in the environments with the high spatial heterogeneity in the topography, forest type, tree species composition, and so on, and addressing physiological responses of trees and stands to specific environmental controls. Meanwhile, Ford et al. (2007) and Oishi et al. (2008) indicated that the accuracy of ET_{com} is greatly affected by the sap flow upscaling procedure, while the largest source of variability in the upscaling procedure is landscape variation in stand density and sapwood area.

In this study, a sap flow upscaling procedure aiming at mixed forest canopy transpiration estimate was established. Compared with the upscaling procedures used in most previous studies, this upscaling procedure was carefully refined, and accounted for the diversities of forest types and tree species. With the using of this carefully refined sap flow upscaling procedure, although the number of the experimental trees in this study was relatively small, the representativeness of ET_{com} for large spatial scales was relatively good. The ET_{com} based on this refined sap flow upscaling procedure was well matched with ET_{ec}, and both of them were then believed to be relatively accurate. As mentioned before, in this study, the net annual changes in catchment water storage were

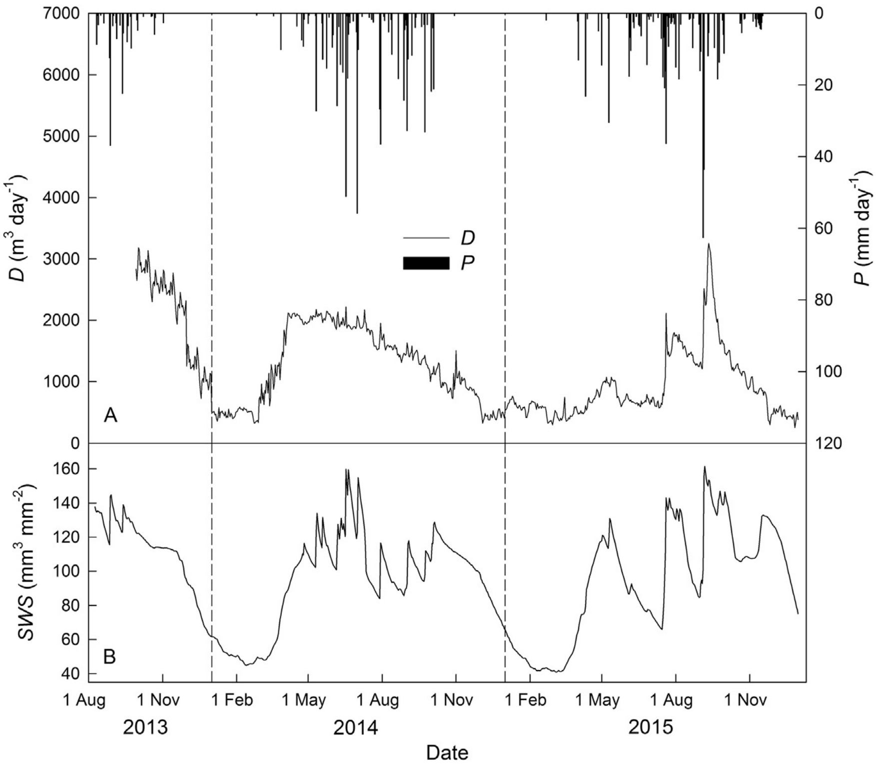

Fig. 3. Seasonal variations in the daily values of (A) discharge (D) and precipitation (P), and (B) soil water storage (SWS) of 0–850 mm soil layer in 2013, 2014 and 2015.

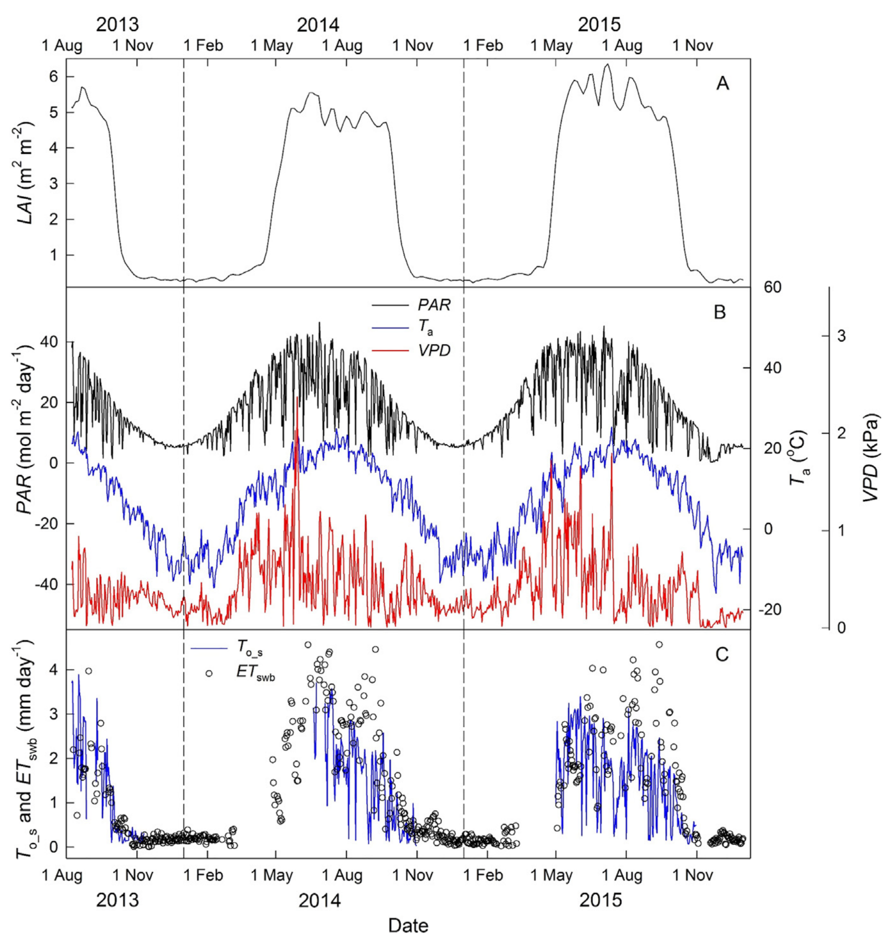

Fig. 4. Seasonal variations in the daily values of (A) leaf area index (LAI), (B) photosynthetically active radiation (PAR), air temperature (T_a), and vapor pressure deficit (VPD), and (C) overstory canopy transpiration estimates from sap flow (T_{o_s}) and entire ecosystem evapotranspiration estimates from soil water budget (ET_{swb}) in 2013, 2014 and 2015.

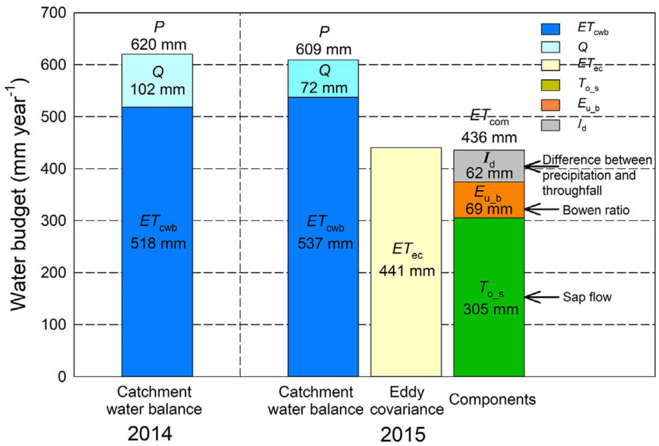

Fig. 5. The left two bars show annual estimates of entire ecosystem evapotranspiration from catchment water balance (ET_{cwb}) in 2014 and 2015, and the right two bars show annual estimates of entire ecosystem evapotranspiration from eddy covariance (ET_{ec}) and as the sum of evapotranspiration components (ET_{com}) in 2015. Annual ET_{cwb} is estimated as the residual of total annual precipitation (P) minus total annual runoff (Q). Annual ET_{com} is estimated as the sum of total annual estimates of overstory canopy transpiration from sap flow (T_{o_s}), of understory vegetation evapotranspiration from Bowen ratio-energy balance (E_{u_b}), and of overstory canopy interception loss as the difference between precipitation and throughfall (I_d).

not taken into consideration in the catchment water balance method, and the energy imbalance correction was not conducted for the eddy covariance method. As a matter of fact, even after accounting for the measured net annual change in *SWS* and the energy imbalance correction for eddy covariance flux, ET_{cwb} (528 mm) was still markedly higher than ET_{ec} (492 mm), further verifying that ET_{cwb} was quite likely to overestimate annual *ET*. As introduced in Section 2.1, XEW is a typical area of the earth-rock-mixed mountainous region of North China, and according to the field geological investigations conducted in XEW, regolith and fractured bedrock are widely distributed under the ground. Therefore, bedrock infiltration and deep drainage might not be negligible, and groundwater flow in XEW might be quite abundant. Katsuyama et al. (2010) also pointed out that bedrock infiltration is not negligible under some geological conditions. The long-periodic stable isotope analyses on the rainwater, soil water, groundwater, and streamwater, which was conducted in XEW, also supported the viewpoint that bedrock infiltration and deep drainage is not negligible in this watershed. Because *Q* measured by the weir in the catchment water balance method was only the surface runoff, and the subsurface runoff could not be measured, non-negligible subsurface runoff might lead to significant underestimate of *R*, then resulting in overestimate of *ET* using the catchment water balance method. As a consequence, it was thought that the catchment water balance method might be not applicative and reliable in the forest catchments with similar geologic and hydrologic conditions. Furthermore, according to the annual *ET* results of the previous studies shown in Table 4, ET_{cwb} is, to different extent, higher than ET_{ec} and ET_{com} in the most of these studies, which effectively supports the conclusion drawn in this study that the catchment water balance method probably overestimates *ET*.

Partitioning *ET* into T_o, E_u, and *I* is critical for understanding the water cycle and linked ecological processes (Good et al., 2015). In this study, the fractions of the *ET* components contributing to *ET* at annual scale were respectively 70% (T_{o_s}/ET_{com}), 16% (E_{u_b}/ET_{com}), and 14% (I_d/ET_{com}). The annual transpiration ratio (T_o/ET) was relatively higher than that in other studies in Table 4, which might result from the high forest coverage of XEW, quite closed overstory canopy in summer, and cold and dry weather in winter.

Furthermore, it was worth noting that, as the time series of the annual *ET* and its components in this study was relatively short, only some qualitative analyses were conducted at annual scale, and the persuasiveness of the conclusions drawn above at annual scale was relatively limited. More and deeper analyses could be carried out at monthly, daily, and diurnal scales in the next several sections.

3.3. Comparisons at the monthly scale

To further evaluate the reliabilities of ET_{ec} and ET_{com}, and to detect the controlling factors of *ET* and its components, monthly ET_{ec} and ET_{com} in 2014 and 2015 are depicted in Fig. 6, and the *ET* components estimates and several physiological and environmental factors are also shown. Fig. 6 shows quite good agreement between ET_{ec} and ET_{com} at monthly scale, and the differences between the two estimates are quite slight for most of the months during the experimental period, further validating the reliabilities of both *ET* estimation methods. It should be noted that sap flow was only measured during the growing season (from April to October) of the year in this study, while during the rest of the year, according to the field observations, there was nearly no leaf on the trees in XEW, and T_o was then considered to be negligible, which is also a usual practice for the sap flow studies in deciduous forest regions.

As depicted in Fig. 6, the seasonal variation in *ET* is quite significant, while it shows good agreement with the seasonal variations in *LAI* and *PAR*, implying *LAI* and *PAR* are two important affecting factors of *ET* in XEW. *ET* rose to higher than 70 mm month^{-1} in the summer (June, July, and August), while it dropped to lower than 5 mm month^{-1} in the winter (December, January, and February), which might mainly result from the climatic characteristics of the monsoon-influenced subhumid continental climate in XEW (hot/humid summer and cold/dry winter) and the defoliation of the deciduous forest in the winter. As for the *ET* components, *I* showed a quite close relationship with *P*, and E_u was slight during the summer, mainly because the overstory canopy was too thick and closed to allow the solar radiation to pass through and reach the understory vegetation. For the similar reason, the monthly transpiration ratio (T_o/ET) was quite high in the summer, and T_{o_s}/ET_{com} even reached 85% in some months. Moreover, the E_u in April, September, and October was obviously higher than that in the other months of the year, for the reason that in these three months, the overstory canopy was relatively thin compared with that in the summer, and the solar radiation then could pass through the overstory canopy and reach the understory vegetation, meanwhile, T_a, *PAR*, and *VPD* were relatively high compared with those in the winter, which might effectively promote soil evaporation and vegetation transpiration.

3.4. Comparisons at the daily scale

Daily variations in ET_{ec}, T_{o_s}, E_{u_b}, and ET_{swb} in 2014 and 2015 are depicted in Fig. 7, the seasonal trends and the daily fluctuations of them are shown. Moreover, the correlation analyses were conducted between ET_{swb} and ET_{ec}, and between ET_{com} and ET_{ec} at daily scale, and the relationships of daily ET_{swb} and ET_{com} against ET_{ec} in 2015 are scatter-plotted in Fig. 8. Linear regression analyses were carried out (see Fig. 8 for detailed results), and the slopes of the regression lines are 0.8847 ($r^2 = 0.4608$) and 0.9357 ($r^2 = 0.7058$) respectively for ET_{swb} and ET_{com} against ET_{ec}.

Fig. 7 exhibits that the day-to-day fluctuations in ET_{ec} and T_{o_s} are quite large, while their fluctuations are matched. In the summer, T_o accounted for the principal part of *ET*. According to Fig. 8, at daily scale, the correlation between ET_{com} and ET_{ec} is quite significant, and the slope of the regression line is fairly close to 1, revealing satisfactory agreement between daily ET_{com} and ET_{ec}, which is consistent with the results acquired at annual and monthly scales, and further verifies the accuracies of these two *ET* estimation methods. The figures also show significant correlation between daily ET_{swb} and ET_{ec}, and the day-to-day fluctuation in ET_{swb} qualitatively coincides with that in ET_{ec}. It was noteworthy that the slope of the linear regression line between daily ET_{swb} and ET_{ec} in Fig. 8 was, to a certain extent, lower than 1, which

Table 4
Comparison of annual evapotranspiration and its components estimated by different methods from published studies in comparable forests and from this study.

Site description	Catchment area (km^2)	Year	P	Q	T_o[a]	E_u	I	ET_{cwb}[b]	ET_{ec}	ET_{com}	Reference
• 35°57′30″ N, 84°17′15″ W	0.98	1995						~593	~538		Wilson et al.
• Mixed deciduous broad-leaved forest		1996						~641	~554		(2001)
• Upland		1997						~534	~612		
• Well drained soil classified as typic Paleudult (encompasses clayey		1998	1225	723	230	86	104	502	547	420	
and kaolinitic soils)		1999	1152	510	269	91	105	642	605	465	
• Annual maximum leaf area index: about 6 $m^2\ m^{-2}$											
• 36°58′41.430″ N, 79°05′39.087″ W		2002	1092		336	84	189		577	610	Oishi et al.
• Mixed deciduous broad-leaved forest (evergreen coniferous		2003	1346		329	102	236		618	668	(2008)
species make up a minor component)		2004	992		346	108	181		618	635	
• Flat topography with <4% slope		2005	934		343	119	157		605	619	
• Soil classified as Iredell gravely loam (a clay pan with low											
hydraulic conductivity at the depth of approximately 35 cm)											
• Soil depth: 2 m											
• Annual maximum leaf area index: 5.9–6.7 $m^2\ m^{-2}$											
• Pure evergreen coniferous forest	0.14	2004	2160	655	726		566	1505		1292[c]	Ford et al.
• Steeply sloping (about 57% slope)		2005	2321	928	686		604	1392		1290[c]	(2007)
• Bedrock property: impenetrable											
• Annual maximum leaf area index: 9.35–14.18 $m^2\ m^{-2}$											
• 33°08′ N, 130°43′ E	0.04	2007	~1953	~1122	359[d]	127[d]	425[d]	831	707	911[d]	Shimizu et al.
• Mixed evergreen coniferous forest (deciduous broad-leaved									840[e]		(2015)
species make up a minor component)		2008	~2200	~1084				1116	712		
• Steeply sloping (36–84% slope)									812[e]		
• Soil depth: typically around 1 m											
• Bedrock property: crystalline schist											
• Annual maximum leaf area index: 5.4–5.9 $m^2\ m^{-2}$											
• Mixed evergreen coniferous forest		2003/2004[f]	231		134	99	27		235	260	Yaseef et al.
• Rocky hillslope		2004/2005[f]	377		156	112	39		343	307	(2010)
• Soil classified as loess of aeolian-origin (with clay-loam texture)		2005/2006[f]	224		111	93	26		227	230	
• Soil depth: 0.2–0.4 m		2006/2007[f]	308		115	106	33		263	254	
• Bedrock property: chalk and limestone (some fractured)											
• Deep groundwater (>300 m)											
• Annual maximum leaf area index: 1.50 $m^2\ m^{-2}$											
• 34°58′ N, 136°00′ E	0.06	2001	1438	699				739	720[e]		Kosugi and
• Mixed evergreen coniferous forest (deciduous broad-leaved		2002	1179	405				774	735[e]		Katsuyama
species make up a minor component)		2003	1971	1098				873	750[e]		(2007)
• Slightly sloping (about 16% slope)											
• Soil classified as brown forest soil											
• Bedrock property: weathered granite with considerable amounts											
of albite											
• Annual maximum leaf area index: 5.5 $m^2\ m^{-2}$											
• 25°21′ N		2004	1320		872				1378[e]		Krauss et al.
• Riverine mixed mangrove forest		2005[g]	779		664				1007[e]		(2015a)
• Close to river mouth											
• This study	4.22	2014	620	102				518			This study
		2015	609	72	305	69	62	537	441	436	

Annual values of precipitation (P); runoff (Q); transpiration of the overstory canopy (T_o); evapotranspiration from the understory vegetation, including soil evaporation and the transpiration of the understory vegetation (E_u); interception loss of the overstory canopy (I); the entire ecosystem evapotranspiration estimated from the catchment water balance method (ET_{cwb}); the entire ecosystem evapotranspiration estimated from the eddy covariance method (ET_{ec}); and the entire ecosystem evapotranspiration estimated as the sum of three evapotranspiration components ($ET_{com} = E_u + T_o + I$). All units are mm $year^{-1}$. Note that numbers with ~ were not the directly reported data, and they are estimated from the figures in the literatures.

[a] All upscaled from sap flow measurement.
[b] All assume negligible net annual change in catchment water storage.
[c] Soil evaporation neglected.
[d] Value from April 2007 to March 2008.
[e] With energy imbalance correction.
[f] From October of the first year to September of the second year.
[g] Data from January 1 to August 31, 2005.

was mainly because I was not contained in ET_{swb}, leading to underestimate of ET using the soil water budget method. The reasonably good agreement between daily ET_{swb} and ET_{ec} indicated that although ET_{swb} had some disadvantages such as poor continuity, relatively high variability, and not containing I, and might be influenced by the lateral flow and deep drainage loss, it could principally reflect the overall trend and the daily dynamics of ET, while the general grasp of ET trend and dynamics was of great importance. However, as elucidated by Wilson et al. (2001), data scatter and excessive missing data during and after the rain events severely limit the applicability of the soil water budget method for estimating annual ET, and some trees may have accessed water beneath the depth of soil water content measurements under severe drought conditions, leading to underestimate of ET using this method.

ET partitioning was also analyzed at the daily scale. The daily T_{o_s}/ET_{ec} and E_{u_b}/ET_{ec} values (with an inverted y-axis scale) in 2014 and 2015 are depicted in Fig. 9, while LAI is also shown in the figure for contrast. It is worth noting that, in Fig. 9, the right y-axis tick mark $E_{u\_b}/ET_{ec} = 0.0$ corresponds to the left y-axis tick mark $T_{o\_s}/ET_{ec} = 1.0$, while the right y-axis tick mark $E_{u\_b}/ET_{ec} = 1.0$ corresponds to the left y-axis tick mark $T_{o\_s}/ET_{ec} = 0.0$. As indicated in Eq. (1) in Section 1, ET is equal to the sum of E_u, T_o, and I. However, I was generated during only rain events and short periods following these events, and I was negligible during rainless days, which were the majority of the days in a year.

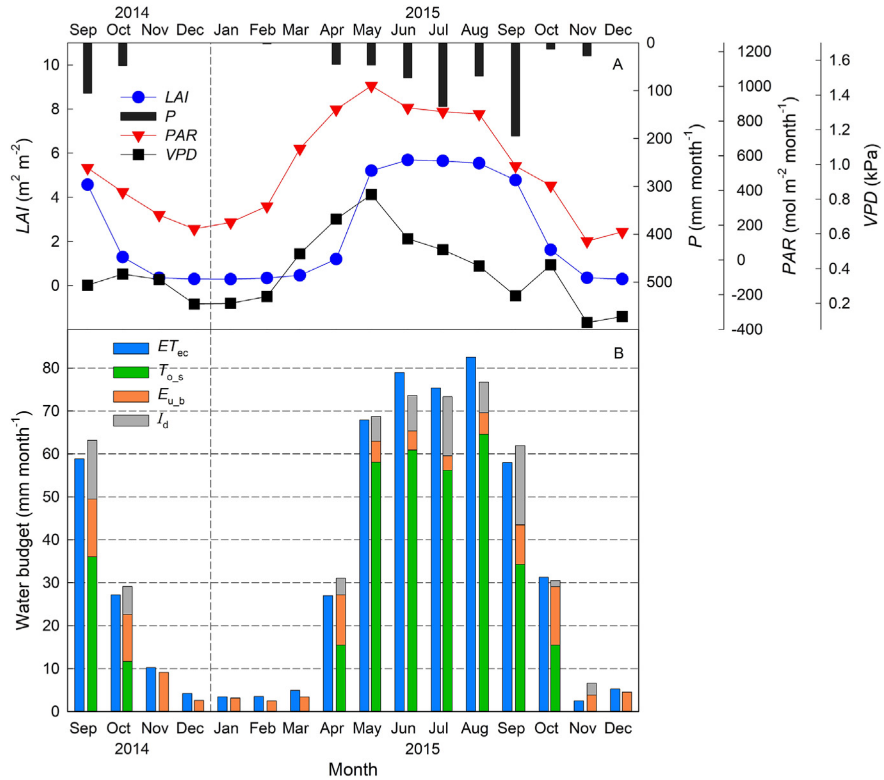

Fig. 6. Monthly (A) leaf area index (*LAI*), precipitation (*P*), photosynthetically active radiation (*PAR*), and vapor pressure deficit (*VPD*), and (B) estimates of entire ecosystem evapotranspiration from eddy covariance (ET_{ec}) and as the sum of evapotranspiration components (ET_{com}) in 2014 and 2015. Monthly ET_{com} is estimated as the sum of monthly estimates of overstory canopy transpiration from sap flow (T_{o_s}), of understory vegetation evapotranspiration from Bowen ratio-energy balance (E_{u_b}), and of overstory canopy interception loss as the difference between precipitation and throughfall (I_d). Note that the value of T_{o_s} in April 2015 was missing, and was approximately estimated using the value of T_{o_s} in October 2015 for the similar values of *LAI* and *PAR* in these two months.

The sum of T_o/ET and E_u/ET might be equal to 1, when I was assumed negligible, implying that the T_o/ET and E_u/ET data points might be coincident depending on the coordinate axis settings in Fig. 9. According to Fig. 9, there are substantial day-to-day fluctuations in both T_{o_s}/ET_{ec} and E_{u_b}/ET_{ec}, while their fluctuations are qualitatively matched, and the T_{o_s}/ET_{ec} and E_{u_b}/ET_{ec} data points are roughly coincident, verifying the reliabilities of these methods for estimating ET and its components from another side. The daily transpiration ratio (T_o/ET, $1 - E_u/ET$) was quite close to 1 during the summer, and dropped to nearly 0 in the winter. The seasonal trend of the daily transpiration ratio (T_o/ET, $1 - E_u/ET$) was quite similar with that of *LAI*, implying that *LAI* was the main controlling factor of the transpiration ratio, which was consistent with the conclusions of Wang et al. (2014) and Wei et al. (2015).

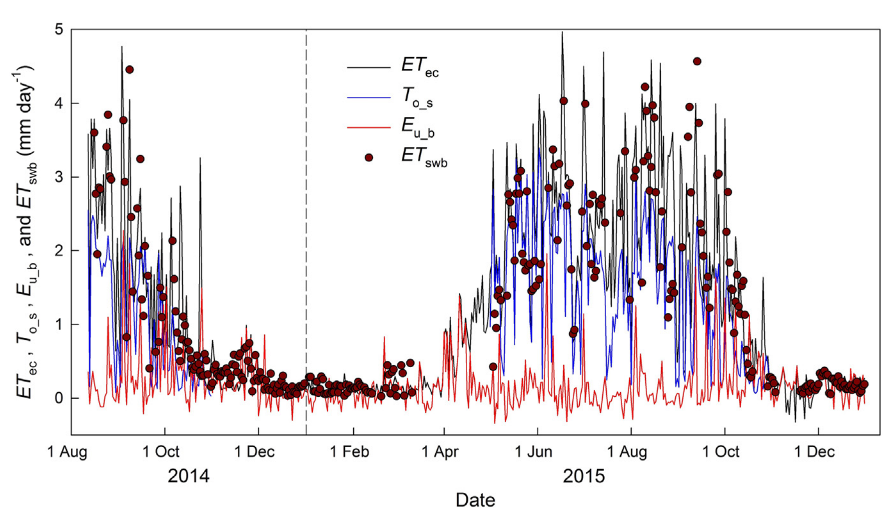

Fig. 7. Daily estimates of entire ecosystem evapotranspiration from eddy covariance (ET_{ec}), of overstory canopy transpiration from sap flow (T_{o_s}), of understory vegetation evapotranspiration from Bowen ratio-energy balance (E_{u_b}), and of entire ecosystem evapotranspiration from soil water budget (ET_{swb}) in 2014 and 2015.

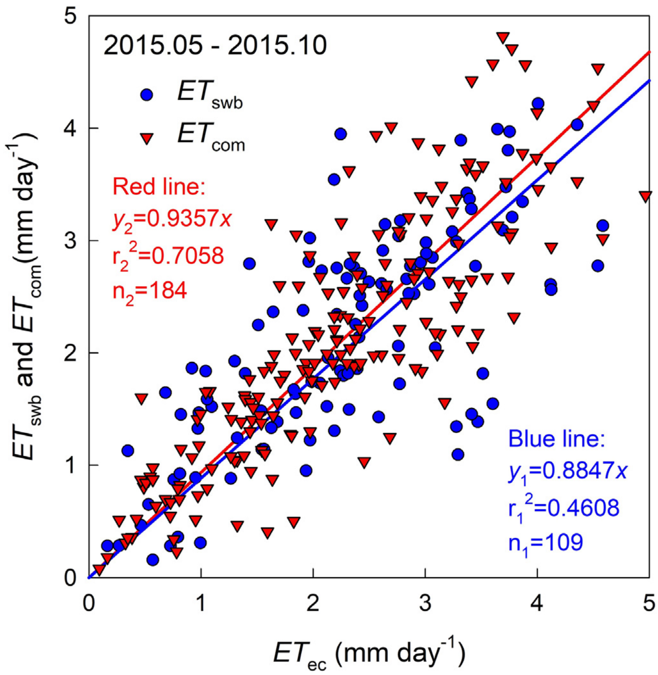

Fig. 8. Daily estimates of entire ecosystem evapotranspiration from soil water budget (ET_{swb}, blue circles) and as the sum of evapotranspiration components (ET_{com}, red triangles) respectively against estimates from eddy covariance (ET_{ec}) in 2015. Regression lines, regression equations, coefficients of determination (r^2), and numbers of data (n) are also shown. Note that the blue line is the regression line between ET_{swb} and ET_{ec}, and the red line is the regression line between ET_{com} and ET_{ec}.

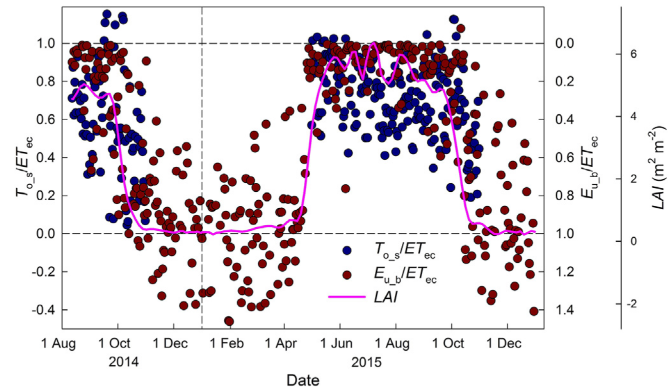

Fig. 9. Daily transpiration ratio (T_{o_s}/ET_{ec}, the ratio of overstory canopy transpiration estimates from sap flow to entire ecosystem evapotranspiration estimates from eddy covariance), the ratio of understory vegetation evapotranspiration estimates from Bowen ratio-energy balance to entire ecosystem evapotranspiration estimates from eddy covariance (E_{u_b}/ET_{ec}, inverted axis scale), and leaf area index (*LAI*) in 2014 and 2015. Note that the right y-axis tick mark $E_{u\_b}/ET_{ec} = 0.0$ corresponds to the left y-axis tick mark $T_{o\_s}/ET_{ec} = 1.0$, while the right y-axis tick mark $E_{u\_b}/ET_{ec} = 1.0$ corresponds to the left y-axis tick mark $T_{o\_s}/ET_{ec} = 0.0$.

3.5. Comparisons at the diurnal scale

The comparison of the different methods for estimating *ET* and its components was also conducted at diurnal scale, and the accuracy of the methods were further evaluated. Averaged diurnal courses of half-hourly T_{o_s} and ET_{ec} as a function of *PAR*, T_a, and *VPD* in 2015 are depicted in Fig. 10. Error bars in the figure represent standard errors ($n = 153$). As shown in the figure, the diurnal course of ET_{ec} roughly matches that of *PAR*, and the variations in ET_{ec} and *PAR* are synchronized at diurnal scale. However, the diurnal course of T_{o_s} pronouncedly lagged behind the diurnal courses of ET_{ec} and *PAR* by a factor of about 1 h, while the diurnal track shapes of T_{o_s}, ET_{ec}, and *PAR* were quite similar. The diurnal peak time of T_{o_s} roughly matched the diurnal peak times of T_a and *VPD*, while the diurnal track shape of T_{o_s} were, to some extent, different from the diurnal track shapes of T_a and *VPD*. Many previous studies analyzed the diurnal time lag between sap flow and environmental factors (Arneth et al., 1996; Bai et al., 2017; Bai et al., 2015; Chen et al., 2014; Chen et al., 2011; O'Brien et al., 2004; O'Grady et al., 2008; Zeppel et al., 2004). Tie et al. (2017) also pointed out that, according to the study conducted in XEW, although *PAR* is identified as the key environmental factor controlling sap flow at daily scale, the variation in sap flow markedly lags behind that in *PAR* at diurnal scale, and it is thought that the diurnal time lag between sap flow and *PAR* mainly contains two parts: the diurnal time lag between sap flow and T_o, and that between T_o and *PAR*.

To further detect the diurnal time phase relations and time lags between the diurnal courses of T_{o_s}, ET_{ec}, and *PAR*, the averaged diurnal hysteresis loops between half-hourly T_{o_s} and *PAR*, between half-hourly ET_{ec} and *PAR*, and between half-hourly T_{o_s} and ET_{ec} in 2015 are shown in Fig. 11. In the figure, the error bars represent the standard errors ($n = 153$), and the arrows denote the rotation directions of the hysteresis loops. As shown in the figure, the diurnal hysteresis loop between T_{o_s} and *PAR* is significant and exhibits a counter clockwise rotation, indicating that the variation in T_{o_s} lags significantly behind that in *PAR*, while the diurnal hysteresis loop between ET_{ec} and *PAR* is slight, indicating that the variation in ET_{ec} is roughly synchronized with that in *PAR*. The diurnal hysteresis loop between T_{o_s} and ET_{ec} was also significant and exhibits a counter clockwise rotation, indicating that the variation in T_{o_s} also lagged significantly behind that in ET_{ec}. Some previous studies also pointed out the diurnal time lag between sap flow and eddy covariance measurements during the comparison of these two methods in the forest, and generally attributed this phenomenon to non-steady-state conditions and time dependent redistribution of water within the trees (Granier et al., 1996; Granier et al., 2000; Hogg et al., 1997).

The deeper mechanism of the diurnal time lag between T_{o_s} and ET_{ec} was then analyzed. Fig. 10 and Fig. 11 plot the averaged diurnal courses and hysteresis loops of all the days from May to September in 2015, and as elucidated in Sections 3.3 and 3.4, during these months, the transpiration ratio (T_o/ET) is close to 1, and T_o overwhelmingly accounts for the principal part of *ET*, which is also confirmed by Fig. 10. Therefore, theoretically, the diurnal courses of T_o and *ET* might be approximately synchronized. ET_{ec} was an estimate of *ET* using the eddy covariance method, and the compensation for time lag was conducted during the data processing procedures in the eddy covariance method, so it was generally believed that the diurnal time lag between ET_{ec} and *ET* was negligible, implying that the diurnal time phase of ET_{ec} could approximately reflect that of T_o. Thus, the slight diurnal hysteresis loop between ET_{ec} and *PAR* indicated that the diurnal time lag between T_o and *PAR* was slight, implying that the response time of T_o to the change in *PAR* was actually very short, while the significant diurnal hysteresis loop between T_{o_s} and ET_{ec} indicated that there was quite significant diurnal time lag between T_{o_s} and T_o. However, T_{o_s} was an estimate of T_o upscaled from stem sap flow measurement, so the diurnal time phases of T_{o_s} and stem sap flow were the same. As a consequence, the significant diurnal time lag between stem sap flow and T_o led to the significant diurnal time lag between T_{o_s} and T_o, which was a critical system error in upscaling stem sap flow to estimate T_o at diurnal scale. It was also proven that the diurnal time lag between stem sap flow and *PAR* found in Tie et al. (2017) mainly resulted from the diurnal time lag between stem sap flow and T_o, rather than that between T_o and *PAR*. The diurnal time lag between stem sap flow and T_o has also been reported and discussed by some previous studies (Granier et al., 2000; Kume et al., 2008; Phillips et al., 1999).

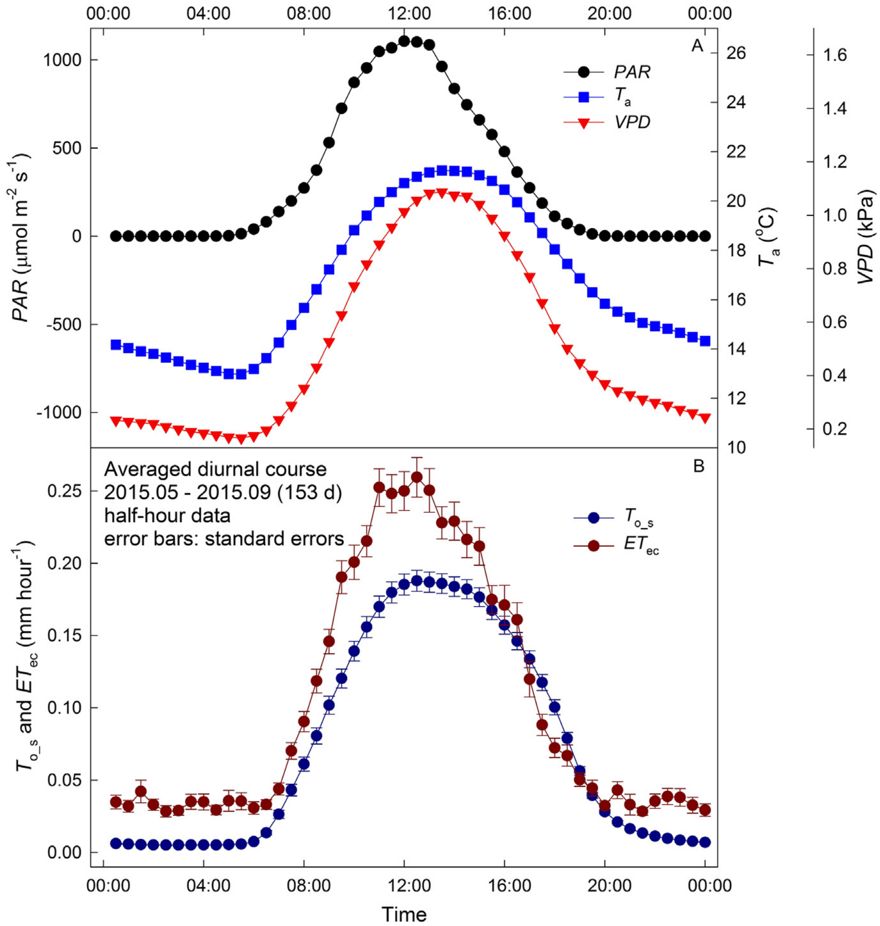

Fig. 10. Averaged diurnal courses of (B) half-hourly mean estimates of overstory canopy transpiration from sap flow (T_{o_s}) and of entire ecosystem evapotranspiration from eddy covariance (ET_{ec}) as a function of (A) photosynthetically active radiation (*PAR*), air temperature (T_a), and vapor pressure deficit (*VPD*) in 2015. Error bars in (B) represent standard errors ($n = 153$).

In addition, the markedly diurnal time lag between stem sap flow and T_o principally resulted from the considerably long response time of stem sap flow to the change in T_o. Chen et al. (2016) simultaneously measured crown and basal stem sap flows of a tree, and found markedly diurnal time lag between them, and pointed out that water storage in the tree stem contributes to the response of tree to the short-term water shortage, and thus has significant impact on the response time of stem sap flow to the change in T_o. The

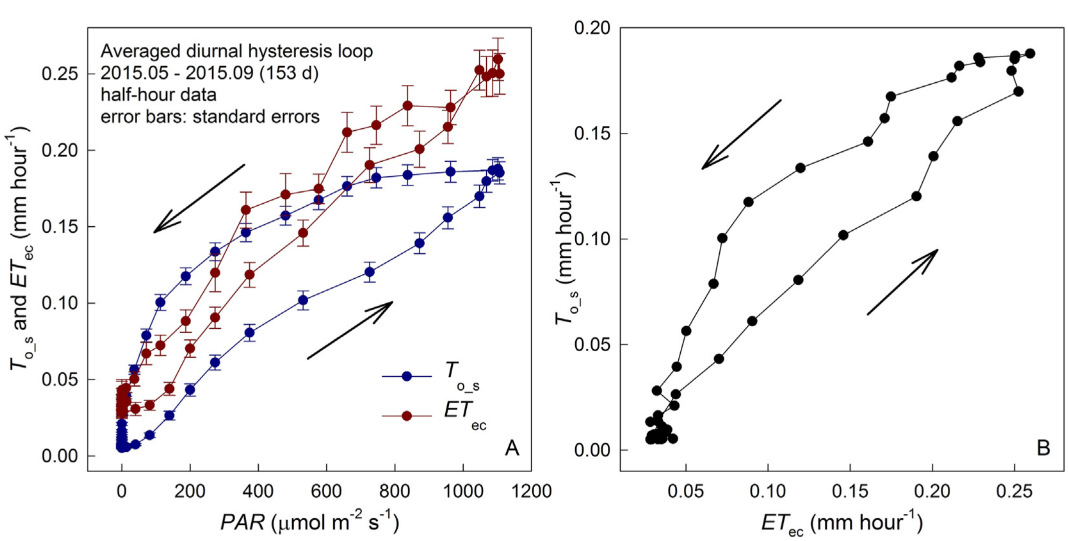

Fig. 11. Averaged diurnal hysteresis loops (A) between half-hourly mean estimates of overstory canopy transpiration from sap flow (T_{o_s}) and photosynthetically active radiation (*PAR*) and between half-hourly mean estimates of entire ecosystem evapotranspiration from eddy covariance (ET_{ec}) and photosynthetically active radiation (*PAR*), and (B) between half-hourly mean estimates of overstory canopy transpiration from sap flow (T_{o_s}) and of entire ecosystem evapotranspiration from eddy covariance (ET_{ec}) in 2015. Error bars in (A) represent standard errors ($n = 153$), and arrows denote the rotation directions of the hysteresis loops.

impact of tree water storage on stem sap flow were also discussed by some other studies (Cermak et al., 2007; Phillips et al., 2003). Moreover, obviously, the hydraulic conductivity and resistance of the tree stem might also control the response time of stem sap flow to the change in T_o. Therefore, to the knowledge of the authors, diurnal time lag between stem sap flow and T_o might be mainly determined by water storage and hydraulic conductivity of tree stem. However, more studies are needed in the future to detect the in-depth physiological mechanism and controlling factors of the diurnal time lag between stem sap flow and T_o, and to establish correction methods in order to eliminate or decrease the system error of time phase in upscaling stem sap flow to estimate T_o at diurnal scale.

4. Conclusions

Several different methods for determining forest evapotranspiration and its components were compared at multiple temporal scales based on in situ observations conducted in a subhumid mountainous catchment covered by mixed deciduous forest in North China. The main findings of this study are summarized as follows:

(1) A sap flow upscaling procedure, accounting for the diversities of forest types and tree species, is established for the mixed deciduous forest. Combining sap flow-based overstory canopy transpiration estimate, Bowen ratio-energy balance-based understory vegetation evapotranspiration estimate, and overstory canopy interception loss estimate, the evapotranspiration of the entire ecosystem is estimated as the sum of the three components, and this estimates agree with the estimates from the eddy covariance method at annual, monthly, and daily temporal scales, although slightly lower in most of the seasons. The reasonably good agreement between the two estimates at multiple temporal scales and the acceptable energy balance closure of the eddy covariance measurement provides confidence in these two approaches for estimating forest evapotranspiration. The estimate from the soil water budget method is also qualitatively similar to the estimates from these two approaches at the daily scale. Although the soil water budget method has some disadvantages such as poor continuity and relatively low precision, it can principally reflect the overall trends and dynamics of forest evapotranspiration.

(2) At the annual scale, the estimate of entire ecosystem evapotranspiration from the catchment water balance method is significantly higher than that from the eddy covariance method, indicating that the catchment water balance method might probably overestimate the annual regional evapotranspiration in this subhumid mountainous forest catchment given our confidence in the eddy covariance method. Because of the widely distributed regolith and fractured bedrock under the ground, groundwater flow in the catchment is probably not negligible, leading to a pronounced underestimation of runoff, and thus, an overestimation of evapotranspiration. The catchment water balance method, which was believed to provide a robust estimate of catchment evapotranspiration in many studies, may not be applicable or reliable in forest catchments with similar geologic and hydrologic conditions.

(3) At the sub-daily scale, the diurnal course of the estimate of overstory canopy transpiration that is upscaled from sap flow measurements significantly lags behind that of the estimate of entire ecosystem evapotranspiration from the eddy covariance method, implying that there is a considerable diurnal time lag between the sap flow-based canopy transpiration estimate and actual canopy transpiration. The diurnal time lag between stem sap flow and canopy transpiration, which should physiologically be determined by water storage and hydraulic conductivity of tree stems, needs careful consideration and possible correction as a system error when stem sap flow measurements are used to estimate canopy transpiration accurately at the diurnal scale in lieu of annual, monthly, and daily scales, especially for forests with relatively high canopy heights and individual tree volumes.

Acknowledgments

This study was supported by the National Natural Science Foundation of China [NSFC91647205], the Ministry of Science and Technology [2016YFC0402701], and the Foundation of State Key Laboratory of Hydroscience and Engineering [2016-KY-03]. The authors thank all the personnel (including but not limited to Yaping Liu, Zhenyang Peng, Qiankun Guo, Sihan Zhao, Ye Liu, Ran Xu, Hao Sheng, and Zhihua He) who worked on the constructions and experiments of the Xitaizi Experimental Watershed for their contributions to this study. The authors also thank the local government of Xitaizi Village for the permission for the experiments.

References

Allen, R.G., Pereira, L.S., Smith, M., Raes, D., Wright, J.L., 2005. FAO-56 dual crop coefficient method for estimating evaporation from soil and application extensions. J. Irrig. Drain. Eng.-ASCE 131, 2–13.

Arneth, A., Kelliher, F.M., Bauer, G., Hollinger, D.Y., Byers, J.N., Hunt, J.E., et al., 1996. Environmental regulation of xylem sap flow and total conductance of *Larix gmelinii* trees in eastern Siberia. Tree Physiol. 16, 247–255.

Bai, Y., Zhu, G., Su, Y., Zhang, K., Han, T., Ma, J., et al., 2015. Hysteresis loops between canopy conductance of grapevines and meteorological variables in an oasis ecosystem. Agric. For. Meteorol. 214–215, 319–327.

Bai, Y., Li, X., Liu, S., Wang, P., 2017. Modelling diurnal and seasonal hysteresis phenomena of canopy conductance in an oasis forest ecosystem. Agric. For. Meteorol. 246, 98–110.

Barr, A.G., Morgenstern, K., Black, T.A., McCaughey, J.H., Nesic, Z., 2006. Surface energy balance closure by the eddy-covariance method above three boreal forest stands and implications for the measurement of the CO_2 flux. Agric. For. Meteorol. 140, 322–337.

Blanken, P.D., Black, T.A., Yang, P.C., Neumann, H.H., Nesic, Z., Staebler, R., et al., 1997. Energy balance and canopy conductance of a boreal aspen forest: partitioning overstory and understory components. J. Geophys. Res.-Atmos. 102, 28915–28927.

Bovard, B.D., Curtis, P.S., Vogel, C.S., Su, H.B., Schmid, H.P., 2005. Environmental controls on sap flow in a northern hardwood forest. Tree Physiol. 25, 31–38.

Cammalleri, C., Rallo, G., Agnese, C., Ciraolo, G., Minacapilli, M., Provenzano, G., 2013. Combined use of eddy covariance and sap flow techniques for partition of ET fluxes and water stress assessment in an irrigated olive orchard. Agric. Water Manag. 120, 89–97.

Cermak, J., Kucera, J., Bauerle, W.L., Phillips, N., Hinckley, T.M., 2007. Tree water storage and its diurnal dynamics related to sap flow and changes in stem volume in old-growth Douglas-fir trees. Tree Physiol. 27, 181–198.

Chen, J., Jönsson, P., Tamura, M., Gu, Z., Matsushita, B., Eklundh, L., 2004. A simple method for reconstructing a high-quality NDVI time-series data set based on the Savitzky–Golay filter. Remote Sens. Environ. 91, 332–344.

Chen, L., Zhang, Z., Li, Z., Tang, J., Caldwell, P., Zhang, W., 2011. Biophysical control of whole tree transpiration under an urban environment in Northern China. J. Hydrol. 402, 388–400.

Chen, D., Wang, Y., Liu, S., Wei, X., Wang, X., 2014. Response of relative sap flow to meteorological factors under different soil moisture conditions in rainfed jujube (*Ziziphus jujuba* Mill.) plantations in semiarid Northwest China. Agric. Water Manag. 136, 23–33.

Chen, Y.J., Bongers, F., Tomlinson, K., Fan, Z.X., Lin, H., Zhang, S.B., et al., 2016. Time lags between crown and basal sap flows in tropical lianas and co-occurring trees. Tree Physiol. 36, 736–747.

Chi, J., Waldo, S., Pressley, S., O'Keeffe, P., Huggins, D., Stöckle, C., et al., 2016. Assessing carbon and water dynamics of no-till and conventional tillage cropping systems in the inland Pacific Northwest US using the eddy covariance method. Agric. For. Meteorol. 218–219, 37–49.

Cristiano, P.M., Campanello, P.I., Bucci, S.J., Rodriguez, S.A., Lezcano, O.A., Scholz, F.G., et al., 2015. Evapotranspiration of subtropical forests and tree plantations: a comparative analysis at different temporal and spatial scales. Agric. For. Meteorol. 203, 96–106.

Cuenca, R.H., Stangel, D.E., Kelly, S.F., 1997. Soil water balance in a boreal forest. J. Geophys. Res.-Atmos. 102, 29355–29365.

Du, S., Wang, Y., Kume, T., Zhang, J., Otsuki, K., Yamanaka, N., et al., 2011. Sapflow characteristics and climatic responses in three forest species in the semiarid Loess Plateau region of China. Agric. For. Meteorol. 151, 1–10.

Etzold, S., Buchmann, N., Eugster, W., 2010. Contribution of advection to the carbon budget measured by eddy covariance at a steep mountain slope forest in Switzerland. Biogeosciences 7, 2461–2475.

Foken, T., Göockede, M., Mauder, M., Mahrt, L., Amiro, B., Munger, W., 2004. Post-field data quality control. Handbook of Micrometeorology, pp. 181–208.

Ford, C.R., Hubbard, R.M., Kloeppel, B.D., Vose, J.M., 2007. A comparison of sap flux-based evapotranspiration estimates with catchment-scale water balance. Agric. For. Meteorol. 145, 176–185.

Fortuniak, K., Pawlak, W., Bednorz, L., Grygoruk, M., Siedlecki, M., Zieliński, M., 2017. Methane and carbon dioxide fluxes of a temperate mire in Central Europe. Agric. For. Meteorol. 232, 306–318.

Friedl, M.A., 1996. Relationships among remotely sensed data, surface energy balance, and area-averaged fluxes over partially vegetated land surfaces. J. Appl. Meteorol. 35, 2091–2103.

Good, S.P., Noone, D., Bowen, G., 2015. WATER RESOURCES. Hydrologic connectivity constrains partitioning of global terrestrial water fluxes. Science 349, 175–177.

Granier, A., 1987. Evaluation of transpiration in a Douglas-fir stand by means of sap flow measurements. Tree Physiol. 3, 309–320.

Granier, A., Biron, P., Kostner, B., Gay, L.W., Najjar, G., 1996. Comparisons of xylem sap flow and water vapour flux at the stand level and derivation of canopy conductance for Scots pine. Theor. Appl. Climatol. 53, 115–122.

Granier, A., Biron, P., Lemoine, D., 2000. Water balance, transpiration and canopy conductance in two beech stands. Agric. For. Meteorol. 100, 291–308.

Hammerle, A., Haslwanter, A., Schmitt, M., Bahn, M., Tappeiner, U., Cernusca, A., et al., 2007. Eddy covariance measurements of carbon dioxide, latent and sensible energy fluxes above a meadow on a mountain slope. Bound.-Layer Meteorol. 122, 397–416.

Heusinger, J., Weber, S., 2017. Surface energy balance of an extensive green roof as quantified by full year eddy-covariance measurements. Sci. Total Environ. 577, 220–230.

Hogg, E.H., Black, T.A., den Hartog, G., Neumann, H.H., Zimmermann, R., Hurdle, P.A., et al., 1997. A comparison of sap flow and eddy fluxes of water vapor from a boreal deciduous forest. J. Geophys. Res. Atmos. 102, 28929–28937.

Hu, S., Yu, J., Hu, K., Jin, M., 2010. Impacts of Chinese Pine (*Pinus tabulaeformis*) plantations on rainfall redistribution processes: a case study for the mountainous area of North China. Acta Ecol. Sin. 30, 1751–1757.

Iida, Si, Ohta, T., Matsumoto, K., Nakai, T., Kuwada, T., Kononov, A.V., et al., 2009. Evapotranspiration from understory vegetation in an eastern Siberian boreal larch forest. Agric. For. Meteorol. 149, 1129–1139.

Jasechko, S., Sharp, Z.D., Gibson, J.J., Birks, S.J., Yi, Y., Fawcett, P.J., 2013. Terrestrial water fluxes dominated by transpiration. Nature 496, 347–350.

Katsuyama, M., Tani, M., Nishimoto, S., 2010. Connection between streamwater mean residence time and bedrock groundwater recharge/discharge dynamics in weathered granite catchments. Hydrol. Process. 24, 2287–2299.

Kljun, N., Calanca, P., Rotach, M.W., Schmid, H.P., 2004. A simple parameterisation for flux footprint predictions. Bound.-Layer Meteorol. 112, 503–523.

Kormann, R., Meixner, F.X., 2001. An analytical footprint model for non-neutral stratification. Bound.-Layer Meteorol. 99, 207–224.

Kosugi, Y., Katsuyama, M., 2007. Evapotranspiration over a Japanese cypress forest. II. Comparison of the eddy covariance and water budget methods. J. Hydrol. 334, 305–311.

Kosugi, Y., Takanashi, S., Tanaka, H., Ohkubo, S., Tani, M., Yano, M., et al., 2007. Evapotranspiration over a Japanese cypress forest. I. Eddy covariance fluxes and surface conductance characteristics for 3 years. J. Hydrol. 337, 269–283.

Krauss, K.W., Barr, J.G., Engel, V., Fuentes, J.D., Wang, H., 2015a. Approximations of stand water use versus evapotranspiration from three mangrove forests in southwest Florida, USA. Agric. For. Meteorol. 213, 291–303.

Krauss, K.W., Duberstein, J.A., Conner, W.H., 2015b. Assessing stand water use in four coastal wetland forests using sapflow techniques: annual estimates, errors and associated uncertainties. Hydrol. Process. 29, 112–127.

Kumagai, To, Saitoh, T.M., Sato, Y., Takahashi, H., Manfroi, O.J., Morooka, T., et al., 2005. Annual water balance and seasonality of evapotranspiration in a Bornean tropical rainforest. Agric. For. Meteorol. 128, 81–92.

Kume, T., Komatsu, H., Kuraji, K., Suzuki, M., 2008. Less than 20-min time lags between transpiration and stem sap flow in emergent trees in a Bornean tropical rainforest. Agric. For. Meteorol. 148, 1181–1189.

Levia, D.F., Germer, S., 2015. A review of stemflow generation dynamics and stemflow-environment interactions in forests and shrublands. Rev. Geophys. 53, 673–714.

Liang, W., Ding, G., Zang, Y., Gao, G., Bao, Y., An, Y., et al., 2012. Study on effect of *Pinus tabulaeformis* plantation on rainfall redistribution processes in the mountainous area of North China. Res. Soil Water Conserv. 19, 77–80.

Liu, H., Tian, F., Hu, H.C., Hu, H.P., Sivapalan, M., 2013. Soil moisture controls on patterns of grass green-up in Inner Mongolia: an index based approach. Hydrol. Earth Syst. Sci. 17, 805–815.

Mauder, M., Cuntz, M., Drüe, C., Graf, A., Rebmann, C., Schmid, H.P., et al., 2013. A strategy for quality and uncertainty assessment of long-term eddy-covariance measurements. Agric. For. Meteorol. 169, 122–135.

Mitchell, S.R., Emanuel, R.E., McGlynn, B.L., 2015. Land–atmosphere carbon and water flux relationships to vapor pressure deficit, soil moisture, and stream flow. Agric. For. Meteorol. 208, 108–117.

Moncrieff, J.B., Massheder, J.M., deBruin, H., Elbers, J., Friborg, T., Heusinkveld, B., et al., 1997. A system to measure surface fluxes of momentum, sensible heat, water vapour and carbon dioxide. J. Hydrol. 189, 589–611.

Moncrieff, J., Clement, R., Finnigan, J., Meyers, T., 2004. Averaging, detrending, and filtering of eddy covariance time series. Handbook of Micrometeorology, pp. 7–31.

Murray, T., Verhoef, A., 2007. Moving towards a more mechanistic approach in the determination of soil heat flux from remote measurements. Agric. For. Meteorol. 147, 88–97.

Nagler, P., Scott, R., Westenburg, C., Cleverly, J., Glenn, E., Huete, A., 2005. Evapotranspiration on western U.S. rivers estimated using the Enhanced Vegetation Index from MODIS and data from eddy covariance and Bowen ratio flux towers. Remote Sens. Environ. 97, 337–351.

Naithani, K.J., Baldwin, D.C., Gaines, K.P., Lin, H., Eissenstat, D.M., 2013. Spatial distribution of tree species governs the spatio-temporal interaction of leaf area index and soil moisture across a forested landscape. PLoS One 8, 1–12.

Norman, J.M., Campbell, G., 1998. An Introduction to Environmental Biophysics.

O'Brien, J.J., Oberbauer, S.F., Clark, D.B., 2004. Whole tree xylem sap flow responses to multiple environmental variables in a wet tropical forest. Plant Cell Environ. 27, 551–567.

O'Grady, A.P., Worledge, D., Battaglia, M., 2008. Constraints on transpiration of *Eucalyptus globulus* in southern Tasmania, Australia. Agric. For. Meteorol. 148, 453–465.

Oishi, A.C., Oren, R., Stoy, P.C., 2008. Estimating components of forest evapotranspiration: a footprint approach for scaling sap flux measurements. Agric. For. Meteorol. 148, 1719–1732.

Oki, T., Kanae, S., 2006. Global hydrological cycles and world water resources. Science 313, 1068–1072.

Oren, R., Pataki, D.E., 2001. Transpiration in response to variation in microclimate and soil moisture in southeastern deciduous forests. Oecologia 127, 549–559.

Oren, R., Phillips, N., Katul, G., Ewers, B.E., Pataki, D.E., 1998. Scaling xylem sap flux and soil water balance and calculating variance: a method for partitioning water flux in forests. Ann. Sci. Forest. 55, 191–216 EDP Sciences.

Papale, D., Reichstein, M., Aubinet, M., Canfora, E., Bernhofer, C., Kutsch, W., et al., 2006. Towards a standardized processing of Net Ecosystem Exchange measured with eddy covariance technique: algorithms and uncertainty estimation. Biogeosciences 3, 571–583.

Peng, Z., Tian, F., Hu, H., Zhao, S., Tie, Q., Sheng, H., et al., 2016. Spatial variability of soil moisture in a forest catchment: temporal trend and contributors. Forests 7, 154–172.

Perez, P.J., Castellvi, F., Ibanez, M., Rosell, J.I., 1999. Assessment of reliability of Bowen ratio method for partitioning fluxes. Agric. For. Meteorol. 97, 141–150.

Phillips, N., Oren, R., Zimmermann, R., Wright, S.J., 1999. Temporal patterns of water flux in trees and lianas in a Panamanian moist forest. Trees 14, 116–123.

Phillips, N.G., Ryan, M.G., Bond, B.J., McDowell, N.G., Hinckley, T.M., Cermak, J., 2003. Reliance on stored water increases with tree size in three species in the Pacific Northwest. Tree Physiol. 23, 237–245.

Reichstein, M., Falge, E., Baldocchi, D., Papale, D., Aubinet, M., Berbigier, P., et al., 2005. On the separation of net ecosystem exchange into assimilation and ecosystem respiration: review and improved algorithm. Glob. Chang. Biol. 11, 1424–1439.

Savitzky, A., Golay, M.J., 1964. Smoothing and differentiation of data by simplified least squares procedures. Anal. Chem. 36, 1627–1639.

Scott, R.L., 2010. Using watershed water balance to evaluate the accuracy of eddy covariance evaporation measurements for three semiarid ecosystems. Agric. For. Meteorol. 150, 219–225.

Shen, M., Tang, Y., Chen, J., Zhu, X., Zheng, Y., 2011. Influences of temperature and precipitation before the growing season on spring phenology in grasslands of the central and eastern Qinghai-Tibetan Plateau. Agric. For. Meteorol. 151, 1711–1722.

Shimizu, T., Kumagai, To, Kobayashi, M., Tamai, K., Iida, Si, Kabeya, N., et al., 2015. Estimation of annual forest evapotranspiration from a coniferous plantation watershed in Japan (2): comparison of eddy covariance, water budget and sap-flow plus interception loss. J. Hydrol. 522, 250–264.

Silberstein, R., Held, A., Hatton, T., Viney, N., Sivapalan, M., 2001. Energy balance of a natural jarrah (*Eucalyptus marginata*) forest in Western Australia: measurements during the spring and summer. Agric. For. Meteorol. 109, 79–104.

Small, E.E., McConnell, J.R., 2008. Comparison of soil moisture and meteorological controls on pine and spruce transpiration. Ecohydrology 1, 205–214.

Sonohat, G., Balandier, P., Ruchaud, F., 2004. Predicting solar radiation transmittance in the understory of even-aged coniferous stands in temperate forests. Ann. For. Sci. 61, 629–641.

Stoy, P.C., Katul, G.G., Siqueira, M.B.S., Juang, J.-Y., Novick, K.A., McCarthy, H.R., et al., 2006. Separating the effects of climate and vegetation on evapotranspiration along a successional chronosequence in the southeastern US. Glob. Chang. Biol. 12, 2115–2135.

Sun, G., Noormets, A., Chen, J., McNulty, S.G., 2008. Evapotranspiration estimates from eddy covariance towers and hydrologic modeling in managed forests in Northern Wisconsin, USA. Agric. For. Meteorol. 148, 257–267.

Sun, S., Meng, P., Zhang, J., Wan, X., Zheng, N., He, C., 2014. Partitioning oak woodland evapotranspiration in the rocky mountainous area of North China was disturbed by foreign vapor, as estimated based on non-steady-state ^{18}O isotopic composition. Agric. For. Meteorol. 184, 36–47.

Thompson, S.E., Harman, C.J., Konings, A.G., Sivapalan, M., Neal, A., Troch, P.A., 2011a. Comparative hydrology across AmeriFlux sites: the variable roles of climate, vegetation, and groundwater. Water Resour. Res. 47.

Thompson, S.E., Harman, C.J., Troch, P.A., Brooks, P.D., Sivapalan, M., 2011b. Spatial scale dependence of ecohydrologically mediated water balance partitioning: a synthesis framework for catchment ecohydrology. Water Resour. Res. 47.

Tie, Q., Hu, H., Tian, F., Guan, H., Lin, H., 2017. Environmental and physiological controls on sap flow in a subhumid mountainous catchment in North China. Agric. For. Meteorol. 240–241, 46–57.

van Dijk, A., Moene A.F., de Bruin H.A.R., 2004. The principles of surface flux physics: theory, practice and description of the ECPACK library. Internal Rep., Meteorol. and Air Qual. Group. 1. Wageningen Univ., Wageningen, Netherlands, p. 99.

Vickers, D., Mahrt, L., 1997. Quality control and flux sampling problems for tower and aircraft data. J. Atmos. Ocean. Technol. 14, 512–526.

Wang, L., Good, S.P., Caylor, K.K., 2014. Global synthesis of vegetation control on evapotranspiration partitioning. Geophys. Res. Lett. 41, 6753–6757.

Wang, S., Pan, M., Mu, Q., Shi, X., Mao, J., Brümmer, C., et al., 2015. Comparing evapotranspiration from eddy covariance measurements, water budgets, remote sensing, and land surface models over Canada. J. Hydrometeorol. 16, 1540–1560.

Webb, E.K., Pearman, G.I., Leuning, R., 1980. Correction of flux measurements for density effects due to heat and water-vapor transfer. Q. J. R. Meteorol. Soc. 106, 85–100.

Wei, X., Liu, S., Zhou, G., Wang, C., 2005. Hydrological processes in major types of Chinese forest. Hydrol. Process. 19, 63–75.

Wei, Z., Yoshimura, K., Okazaki, A., Kim, W., Liu, Z., Yokoi, M., 2015. Partitioning of evapotranspiration using high-frequency water vapor isotopic measurement over a rice paddy field. Water Resour. Res. 51, 3716–3729.
Wei, Z.W., Yoshimura, K., Wang, L.X., Miralles, D.G., Jasechko, S., Lee, X.H., 2017. Revisiting the contribution of transpiration to global terrestrial evapotranspiration. Geophys. Res. Lett. 44, 2792–2801.
Williams, D.G., Cable, W., Hultine, K., Hoedjes, J.C.B., Yepez, E.A., Simonneaux, V., et al., 2004. Evapotranspiration components determined by stable isotope, sap flow and eddy covariance techniques. Agric. For. Meteorol. 125, 241–258.
Wilson, K.B., Hanson, P.J., Mulholland, P.J., Baldocchi, D.D., Wullschleger, S.D., 2001. A comparison of methods for determining forest evapotranspiration and its components: sap-flow, soil water budget, eddy covariance and catchment water balance. Agric. For. Meteorol. 106, 153–168.
Wilson, K., Goldstein, A., Falge, E., Aubinet, M., Baldocchi, D., Berbigier, P., et al., 2002. Energy balance closure at FLUXNET sites. Agric. For. Meteorol. 113, 223–243.
Wohlfahrt, G., Hammerle, A., Niedrist, G., Scholz, K., Tomelleri, E., Zhao, P., 2016. On the energy balance closure and net radiation in complex terrain. Agric. For. Meteorol. 226–227, 37–49.
Wullschleger, S.D., Hanson, P.J., Todd, D.E., 2001. Transpiration from a multi-species deciduous forest as estimated by xylem sap flow techniques. For. Ecol. Manag. 143, 205–213.
Xiao, Y., Chen, L., Yu, X., 2007. Characteristics of precipitation redistribution and stemflow in *Quercus acutissima* mixed forest in Miyun, Beijing. J. Northeast Forest. Univ. 8, 006.
Yaseef, N.R., Yakir, D., Rotenberg, E., Schiller, G., Cohen, S., 2010. Ecohydrology of a semi-arid forest: partitioning among water balance components and its implications for predicted precipitation changes. Ecohydrology 3, 143–154.
Zeppel, M.J.B., Murray, B.R., Barton, C., Eamus, D., 2004. Seasonal responses of xylem sap velocity to VPD and solar radiation during drought in a stand of native trees in temperate Australia. Funct. Plant Biol. 31, 461–470.
Zhang, B., Kang, S., Li, F., Zhang, L., 2008. Comparison of three evapotranspiration models to Bowen ratio-energy balance method for a vineyard in an arid desert region of northwest China. Agric. For. Meteorol. 148, 1629–1640.
Zhang, Z., Tian, F., Hu, H., Yang, P., 2014. A comparison of methods for determining field evapotranspiration: photosynthesis system, sap flow, and eddy covariance. Hydrol. Earth Syst. Sci. 18, 1053–1072.
Zhang, Q., Sun, R., Jiang, G., Xu, Z., Liu, S., 2016. Carbon and energy flux from a *Phragmites australis* wetland in Zhangye oasis-desert area, China. Agric. For. Meteorol. 230–231, 45–57.
Zhao, Y., Zhang, M.X., Cao, H.W., Yu, X.X., Liu, B., Zhu, S.B., et al., 2015. Effect of climatic change and afforestation on water yield in the Rocky Mountain Area of North China. Forest Syst. 24, 1–9.
Zhou, Y., Xiao, X., Wagle, P., Bajgain, R., Mahan, H., Basara, J.B., et al., 2017. Examining the short-term impacts of diverse management practices on plant phenology and carbon fluxes of Old World bluestems pasture. Agric. For. Meteorol. 237–238, 60–70.
Ziemblińska, K., Urbaniak, M., Chojnicki, B.H., Black, T.A., Niu, S., Olejnik, J., 2016. Net ecosystem productivity and its environmental controls in a mature Scots pine stand in north-western Poland. Agric. For. Meteorol. 228–229, 60–72.